



Allee effect can simplify the dynamics of a prey-predator model

Partha Sarathi Mandal¹ · Udai Kumar¹ · Koushik Garain¹ · Rakhi Sharma¹

Received: 8 January 2020 / Published online: 24 March 2020

© Korean Society for Informatics and Computational Applied Mathematics 2020

Abstract

In this work, we investigate a prey-predator model which includes the Allee effect phenomena in prey growth function, density dependent death rate for predators and ratio dependent functional response. we fulfill a comprehensive bifurcation analysis, constructing the two-parametric bifurcation diagrams which describes the effect of density dependent death rate parameter, and also show possible phase portraits. We have also investigated the model in the absence of Allee effect and corresponding bifurcation diagram has been presented to show the dynamical changes in the system. Then we compare the properties of the ratio dependent prey-predator model with and without the Allee effect and show that Allee effect has a significant role in the dynamics. Allee effect can preserve local extinction of populations and suppress the stability of interior equilibrium point. Finally, all the analytical results are validated with the help of numerical simulations.

Keywords Prey-predator model · Ratio dependent · Allee effect · Bifurcations · Global dynamics

Mathematics Subject Classification 34C23 · 60J25 · 92D25

1 Introduction

One of the important objectives in population dynamics is to describe the interaction between predator-prey species, represented as the functional response and hence received considerable attentions from several researchers from last few decades. Based on different laboratory experiments, Holling [23] proposed three different types of functional responses like Holling type I, Holling type II and Holling type III to model the phenomena of predation, which made the classical Lotka-Volterra [30,41] sys-

✉ Koushik Garain
koushik.ma18@nitp.ac.in

¹ Department of Mathematics, NIT Patna, Patna, Bihar 800005, India

tem more realistic. Based on these functional responses, a wide variety of dynamical systems ranging from simple two dimensional models to higher dimensional models have been investigated to understand the nature of intersection between prey and predator species within the deterministic environment [16,17,23]. But these modeling approaches are also unable to capture many important ecological factors like difficulties in mate finding, inbreeding depression, food exploitation, predator avoidance or defense etc. [13,40] and most important one is Allee-effect, which was first introduced by Allee [2]. There are two types of Allee effect, one is strong Allee effect and another is weak Allee effect. The strong Allee effect refers to the negative per capita growth rate when population density is below a threshold value and the growth rate is positive when the population density is above this threshold value [42,44]. When the per capita growth rate is decreasing but remains positive, the Allee effect is called weak Allee effect. During last few decades, several mathematical models with Allee effect phenomena have been investigated and it was observed that model with Allee effect have very rich dynamics compared to the analogous models with logistic growth function [18,21,22,33,38,45]. Hence, we study here a prey-predator model with strong Allee effect in prey growth function, whose dynamical analysis is known with logistic prey growth function.

A classical Gauss type predator-prey model is given by the following system of ODEs [17]:

$$\begin{aligned}\frac{dx(t)}{dt} &= x(t)\Psi(x(t), K) - \Phi(x(t))y(t), \\ \frac{dy(t)}{dt} &= y(t)(s\Phi(x(t)) - \gamma),\end{aligned}$$

where $\Phi(x(t))$ is the functional response function, $x(t) > 0$ and $y(t) > 0$ denote, respectively, the population densities of prey and predator species at time 't', $K > 0$ is the carrying capacity of the prey and $\gamma > 0$ is the death rate of the predator. The function $\Psi(x(t), K)$ represents the specific growth rate of the prey in the absence of predator. The simplest form of the function $\Psi(x(t), K)$ commonly used in mathematical modeling of population dynamics is the logistic growth function which has the expression of the form $\Psi(x(t), K) = r\left(1 - \frac{x(t)}{K}\right)$, where r is the maximum relative growth rate and K is the prey carrying capacity. For different mathematical representations of the functional response, readers are referred to [8,12,14,17,23,33].

Holling type I (or Lotka-Volterra) functional response is the basic functional response, which is passing through the origin and unbounded and it is used to model the behavior of passive predators such as spiders. But, the more reasonable functional response will be nonlinear and bounded. In case of Holling type II functional response, the predator grows at a maximum relative growth rate α at high prey population density, whereas at low prey densities Φ approximates the Lotka-Volterra model, asymptotically (as $\Phi \rightarrow \frac{\alpha x}{m}$ when prey density x is at very low level) i.e. predators using this type of functional response cause maximum mortality at low prey density. On the other hand, Holling type III represents a sigmoid growth curve, where it's behavior at low prey population densities becomes quadratic instead of linear, in the

number of prey ($\Phi \rightarrow \frac{\alpha x^2}{m}$ when prey density x is at very low level). In other words, the number of prey attacked per predator increases at an increasing rate at low prey densities, but at a decreasing rate at higher densities until it levels off. If the predators are more efficient at higher prey densities and less efficient at lower prey densities, then the dynamics of the ecosystem is better described by the Holling type III functional response. The Holling type III functional response is useful to model vertebrate predators rather than insects [3] or microbes [11], which are often modeled by the Holling type II response. But it is observed in various studies [9,24,25,28] that there are several circumstances, especially when predators have to search, share, and strive for food, the above functional responses will not be appropriate to model the dynamics of predator-prey interaction and in this case the more suitable functional response is ratio-dependent functional response which is a particular case of so-called predator-dependent functional responses. For this type of functional response, the per capita growth rate for predator should be a function of the ratio of prey to predator abundance. The ratio-dependent functional response was first introduced by Arditi and Ginzburg in [5]. They used the graphical method to analyze their model and concluded that ratio-dependent functional response is a simple way of accounting many types of heterogeneity that happens in large-scale ecological systems, while the prey-dependent form may be more befitting for homogeneous system like chemostats and this was proved through laboratory experiments also [4,19].

Several researchers have studied ratio-dependent functional response in mathematical modelling [6,9,10,15,20,24,25,34,35,38,43]. In 1998, Beretta and Kuang [9] showed that the ratio-dependent models are capable of producing richer and more reasonable or acceptable dynamics and considered time delay. In 2001, authors [10] presented a complete parametric analysis of stability properties and dynamic regimes of an ODE model in which the functional response is a function of the ratio of prey and predator abundances. They showed the existence of eight qualitatively different types of system behaviors realized for various parameter values and they also first demonstrated the complicated analysis of origin in an ecological model. In [6], authors considered spatiotemporal pattern formation in a ratio-dependent predator-prey system and showed that the system can develop patterns both inside and outside of the Turing parameter domain. During 2013, Sen et al. [38] showed that the system exhibits very rich dynamics around non-trivial equilibrium points and system has at most two interior equilibrium points. In 2015, Pallav et al. [35] studied phenomenon of bi-stability, the existence of separatrix curves and several bifurcations such as Hopf bifurcation, saddle-node bifurcation, homoclinic bifurcation and Bogdanov-Takens bifurcation. In most of the cases ratio dependent term is linear but few researchers considered ratio-dependent predator-prey model with Holling type III functional response. In 2004, Wang and Li [43] established the existence of positive periodic solutions for a delayed ratio-dependent predator-prey model with Holling type III functional response and the permanence of the system was also considered. In [15], Fan and Li established the condition for the permanence in a delayed discrete predator-prey model with Holling type III functional response.

We consider here continuous time predator-prey model with Holling type III functional response. On the other hand there are very few works available in the literature

that include the role of density dependent death rate for predators to the system dynamics [7,20,27,32,36,39]. In the past, researchers believed that the density can not affect the growth of a population but the competition among the same species in several natural process suggests the other way. In 2009, Haque [20] considered ratio-dependent predator-prey model with density dependent death rate for predators and found interesting results, they found paradox of enrichment can happen to this system under certain parameter values. As far my knowledge is concerned, nobody has investigated a ratio-dependent prey-predator model with Holling type III functional response and considering both strong Allee effect phenomena in prey growth function and density dependent death rate for predator population. Keeping in mind that, in this work we consider the same model to investigate the influence of Allee effect parameter and density dependent death rate parameter on the dynamics of the system by analyzing the complete stability analysis of the system and global dynamics of the system by performing an extensive bifurcation analysis under several parametric restrictions. Clearly, our work is the extension of the work done in [23,34,35,38]. We show that the conversion rate of prey and death rate of predator have an important role in the dynamics of the system. We also investigate the model without Allee effect and compare the dynamics of the system with Allee model. We show bistability for both Allee model and without Allee model but two coexistence stable steady state is possible for without Allee model at the same time. We find two Bogdanov-Takens bifurcation, two Bautin bifurcation in without Allee model. We show that two transcritical bifurcation curves make the model more complicated. When conversion rate and density independent death rate of predator are equal, stable coexistence state of both the species occur, it can be verify from one parameter bifurcation diagram. In this type of prey-predator model it is very rear to see such complex bifurcation diagram for without Allee model. We show that how stability of origin depends upon the conversion rate of prey, when Allee effect is not present in the system. We show that, Allee effect changes the complicated dynamics of the system to a simple form.

The present work is organized as follows: in Sect. 2, we discuss the basic model with dimensionless variables and parameters and study some basic properties. In Sect. 3, we study the existence and stability of all possible equilibrium points that can occur in the system. Also, we have performed an extensive bifurcation analysis of the system in Sect. 4. It has been observed that the model possesses several types of local bifurcations, namely, saddle-node bifurcation and Hopf-bifurcation, which are of co-dimension one and also the system undergoes one co-dimension two bifurcation, namely, Bogdanov-Takens bifurcation. In Sect. 5, we discuss the global dynamics of the system which includes all possible phase portraits of the system based on the schematic bifurcation diagram. Here, we also proved the existence of one global bifurcation, namely homoclinic bifurcation. In this section, we present another bifurcation diagram with respect to Allee parameter. The system without Allee effect is investigated in Sect. 6. In this section, we present one parameter bifurcation diagram to check the effect of conversion rate, we also compare the dynamics of both the systems with and without Allee effect. In Sect. 7, the chapter is concluded with a brief discussion.

2 Development of the model

In 1989, the general ratio-dependent prey-predator model suggested by Arditi and Ginzburg [5], is

$$\begin{aligned} \frac{dx(t)}{dt} &= rx\Phi(x) - g\left(\frac{x}{y}\right)y, \\ \frac{dy(t)}{dt} &= g\left(\frac{x}{y}\right)y - qy, \end{aligned}$$

where the function $rx\Phi(x)$ is the prey growth in the absence of predators, predator's death rate is represented by qy in the absence of prey and $g\left(\frac{x}{y}\right)$ is the ratio-dependent function. We consider more specific form of this model in the present work by considering strong Allee effect in the prey growth, density dependent death rate for the predator and $g\left(\frac{x}{y}\right) = \frac{x^2}{x^2 + my^2}$. So, we will analyze the following system :

$$\frac{dx}{dt} = rx\left(1 - \frac{x}{k}\right)(x - b) - \frac{\alpha x^2 y}{x^2 + my^2}, \tag{1}$$

$$\frac{dy}{dt} = \frac{\beta x^2 y}{x^2 + my^2} - \gamma y - \delta y^2, \tag{2}$$

subjected to the initial conditions $x(0), y(0) \geq 0$. Here x and y represent prey and predator population density, respectively. The parameters of the system are positive and represented as r is prey intrinsic growth rate, γ is death rate of predator, k is the prey carrying capacity, b is Allee threshold, m is the interference coefficient of predator, α is consumption rate, β is the conversion rate of prey and δ is the predator intra species competition rate. Allee parameter b is defined as $0 < b < k$.

We transform the system $(x, y, t) \rightarrow (u, v, T)$ to a dimensionless form with less number of independent parameters. We use the transformation $x = ku, y = \frac{\beta kv}{\alpha}$, $t = \frac{T}{rb}$ to get the following form:

$$\frac{du}{dT} = u(1 - u)\left(\frac{u}{A} - 1\right) - \frac{Bu^2v}{u^2 + Cv^2} = F_1(u, v), \tag{3}$$

$$\frac{dv}{dT} = \frac{Bu^2v}{u^2 + Cv^2} - Dv - Ev^2 = F_2(u, v), \tag{4}$$

where $A = \frac{b}{k}, B = \frac{\beta}{rb}, C = \frac{m\beta^2}{\alpha^2}, D = \frac{\gamma}{rb}, E = \frac{\beta\delta k}{\alpha rb}$.

2.1 Positivity and boundedness of solution

Any solution starting from the interior of the first quadrant of uv -plane always remain in the first quadrant. So, solution is positive and bounded, proof is similar from [38].

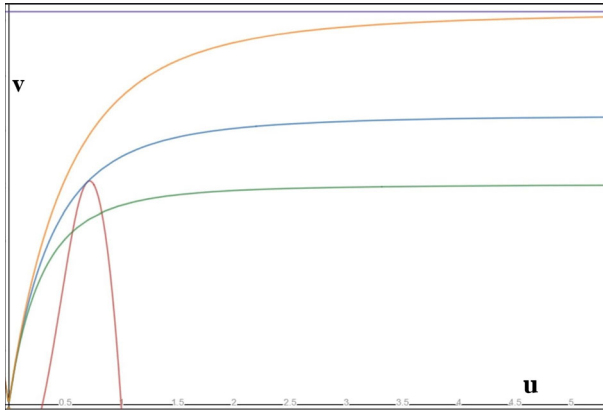


Fig. 1 Possible number of interior equilibrium points changes from zero to two for different values of E . Red coloured curve is the first nullcline and purple coloured line is the asymptote of the second nullcline. Second nullcline is plotted for three different values of E , namely $E = 0.014$ (orange coloured, no interior equilibrium), $E = 0.0190045185$ (blue coloured, saddle-node bifurcation), $E = 0.025$ (green coloured, two interior equilibrium) and other parameters are fixed at $A = 0.3, B = 0.15, C = 0.01, D = 0.1$

3 Equilibrium points and local stability

Here, we examine the existence of possible number of equilibria of the system and their local stability.

3.1 Equilibrium points

The system (3)–(4) has three axial equilibrium points $E_0(0, 0), E_1(A, 0)$ and $E_2(1, 0)$ and the interior equilibrium points are the points of the intersection of the following two non-trivial nullclines:

$$(1 - u) \left(\frac{u}{A} - 1 \right) - \frac{Buv}{u^2 + Cv^2} = 0, \tag{5}$$

$$\frac{Bu^2}{u^2 + Cv^2} - D - Ev = 0. \tag{6}$$

A portion of curve (5) lies in R_+^2 for $u \in [A, 1]$ and it is a continuous smooth curve joining two points $(A, 0)$ and $(1, 0)$ and having a local maximum at u_m such that $A < u_m < 1$ ($0 < A < 1$). The second nullcline (6) intersects the positive u -axis at $(0, 0)$ and then increases monotonically and bounded above by its horizontal asymptote $v = \frac{B-D}{E}$ (see Fig. 1). This observation is true as we assume the restriction $B > D$. But if we consider $B < D$ then nullcline (6) does not have any branch in the positive quadrant of the uv -plane and so the system does not have any feasible interior equilibrium point.

Theorem 3.1 *Let us assume $B > D$ holds. Then the system (3)–(4) admits either no or two interior equilibrium points.*

It is difficult to derive the analytical conditions to determine the number of interior equilibrium points. However, the possible number of feasible interior equilibrium points can be explained from the relative positions and shapes of non-trivial nullclines as presented at Fig. 1. The number of interior equilibrium points can changes from zero to two if we gradually increase the value of the parameter E keeping all other parameters fixed. We assume the u -components of the interior equilibria satisfy the ordering $0 < u_{2*} < u_{1*} < 1$ whenever they exist. In Fig. 1, we have depicted the scenario of changing the number of interior equilibrium points from zero to two with the increasing magnitude of E . In this case we denote two interior equilibrium points, whenever they exist, by $E_{1*}(u_{1*}, v_{1*})$, $E_{2*}(u_{2*}, v_{2*})$ respectively and we find a threshold value of E , which we denote by E_{SN} , where E_{1*} and E_{2*} coincide and one saddle node bifurcation occurs. We study the saddle-node bifurcation in ‘‘Local-bifurcations’’ section in details.

3.2 Local asymptotic stability

Proposition 1 (a) $E_1(A, 0)$ is unstable point if $B > D$ and saddle point if $B < D$.
 (b) $E_2(1, 0)$ is saddle point if $B > D$ and stable point if $B < D$.

Proof The Jacobian matrix of the system (3)–(4) at any point (u, v) is given by,

$$J = \begin{bmatrix} (1-u)(\frac{u}{A}-1) - u(\frac{u}{A}-1) + \frac{u}{A}(1-u) - \frac{2BCuv^3}{(u^2+Cv^2)^2} & \frac{-Bu^2(u^2-Cv^2)}{(u^2+Cv^2)^2} \\ \frac{2BCuv^3}{(u^2+Cv^2)^2} & \frac{Bu^2(u^2-Cv^2)}{(u^2+Cv^2)^2} - D - 2Ev \end{bmatrix}.$$

Taking $T_{11}(u, v) = (1-u)(\frac{u}{A}-1) - u(\frac{u}{A}-1) + \frac{u}{A}(1-u)$, $a_{22}(u, v) = \frac{2BCuv^3}{(u^2+Cv^2)^2}$, $a_{12}(u, v) = \frac{Bu^2(u^2-Cv^2)}{(u^2+Cv^2)^2}$, Jacobian matrix takes the form as following

$$J = \begin{bmatrix} T_{11}(u, v) - a_{22}(u, v) & -a_{12}(u, v) \\ a_{22}(u, v) & a_{12}(u, v) - D - 2Ev \end{bmatrix}.$$

Evaluating the Jacobian matrix at E_1 and E_2 we find,

$$J_{E_1} = \begin{bmatrix} 1-A & 0 \\ -B & B-D \end{bmatrix}, \quad J_{E_2} = \begin{bmatrix} 1-\frac{1}{A} & 0 \\ -B & B-D \end{bmatrix}$$

respectively. As $A < 1$, $E_1(A, 0)$ is a unstable point if $B > D$ and a saddle point if $B < D$. $E_2(1, 0)$ is a saddle point if $B > D$ and a stable point if $B < D$. □

Theorem 3.2 *The origin $E_0(0, 0)$ in (3)–(4) is locally asymptotically stable.*

The Jacobian matrix at $(0, 0)$ have some undefined terms. So we use Blow-up method to determine the stability of equilibrium point $(0, 0)$. Here we use the horizontal Blow-up technique, given by the function $\chi(p, q) = (p, pq) = (u, v)$. Proceeding in a similar fashion like Theorem 3.2 of [1] it can be easily proved that $E_0(0, 0)$ is always locally asymptotically stable.

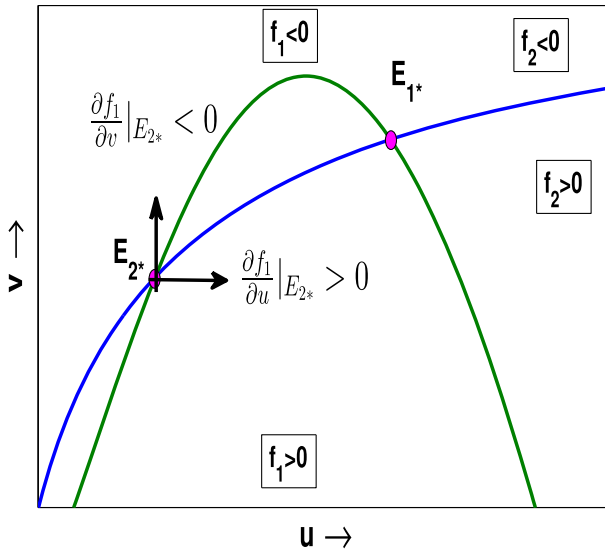


Fig. 2 Green coloured prey nullcline and blue coloured predator nullcline intersect at two interior equilibrium points. Sign of non-trivial nullclines are described in different portions

Proposition 2 Assume that $B > D$ holds.

- (a) E_{1*} is locally asymptotically stable (unstable) if $Tr J_{E_{1*}} < 0$ ($Tr J_{E_{1*}} > 0$).
- (b) E_{2*} is a saddle point whenever it exists.

Proof Let $F_1(u, v) = uf_1(u, v)$ and $F_2(u, v) = vf_2(u, v)$ with $f_1(u, v) = (1 - u)(\frac{u}{A} - 1) - \frac{Buv}{u^2 + Cv^2}$ and $f_2(u, v) = \frac{Bu^2}{u^2 + Cv^2} - D - Ev$. Then we can write,

$$J_{E_{i*}} = \begin{pmatrix} F_{1u} & F_{1v} \\ F_{2u} & F_{2v} \end{pmatrix} = \begin{pmatrix} uf_{1u} & uf_{1v} \\ vf_{2u} & vf_{2v} \end{pmatrix},$$

where $F_{1u} = \frac{dF_1}{du}$ and similar for others. Using the concept of direction field for E_{2*} we find,

$$Sign(J_{E_{2*}}) = Sign \begin{pmatrix} uf_{1u} & uf_{1v} \\ vf_{2u} & vf_{2v} \end{pmatrix} = \begin{pmatrix} + & - \\ + & - \end{pmatrix}.$$

Note that $f_1(u, v) > 0$ for points below the nontrivial prey nullcline and it is positive above it. Hence when we move from left of the equilibria E_{2*} to right sign changes from negative to positive, i.e., $f_1(u_{2*} - \frac{\Delta u}{2}, v_{2*}) < 0$ and $f_1(u_{2*} + \frac{\Delta u}{2}, v_{2*}) > 0$, which imply that $\frac{\partial f_1}{\partial u}|_{E_{2*}} > 0$. Here sign of u_{2*} is positive and hence sign of $u_{2*} \frac{\partial f_1}{\partial u}|_{E_{2*}}$ is positive. Similarly we can found the signs of the other terms of the Jacobian matrix. We provide the graphical representation in Fig. 2. But in this case $\frac{dv^{f_1}}{du}|_{E_{2*}} > \frac{dv^{f_2}}{du}|_{E_{2*}}$, which implies $Det(J_{E_{2*}}) < 0$, so E_{2*} , is always a saddle point. $\frac{dv^{f_1}}{du}$ denotes the slope

of the tangent of the curve $f_1 = 0$ and $\frac{dv(f_2)}{du}$ denotes the slope of the tangent of the curve $f_2 = 0$.

For the equilibrium point E_{1*} , we find

$$Sign(J_{E_{1*}}) = Sign \begin{pmatrix} uf_{1u} & uf_{1v} \\ vf_{2u} & vf_{2v} \end{pmatrix} = \begin{pmatrix} + & - \\ + & - \end{pmatrix}.$$

We have $\frac{dvf_1}{du}|_{E_{1*}} < \frac{dvf_2}{du}|_{E_{1*}}$, which implies $Det(J_{E_{1*}}) > 0$, so E_{1*} is stable if $Tr J_{E_{1*}} < 0$ and unstable if $Tr J_{E_{1*}} > 0$. □

4 Local bifurcations

Here, we investigate that system (3)–(4) exhibits several type of local bifurcations, namely saddle-node bifurcation and Hopf-bifurcation which are of co-dimension one and the system also undergoes co-dimension two bifurcation namely, Bogdanov-Taken bifurcation. Throughout this section we assume that $B > D$ which is necessary for the existence of interior equilibrium points.

4.1 Saddle-node bifurcation

As we discussed above a saddle-node bifurcation occurs in the system (3)–(4) with respect to the parameter E . Two interior equilibrium points $E_{1*}(u_{1*}, v_{1*})$ and $E_{2*}(u_{2*}, v_{2*})$ coincide at a single equilibrium point $E_{SN}^*(u_{sn*}, v_{sn*})$ i.e. two non-trivial nullclines of system (3)–(4) touches each other at $E_{SN}^*(u_{sn*}, v_{sn*})$ at threshold value of E_{SN} . As $F_1(u, v) = uf_1(u, v)$ and $F_2(u, v) = vf_2(u, v)$. Clearly $\frac{dv(f_1)}{du}|_{E_{SN}^*} = \frac{dv(f_2)}{du}|_{E_{SN}^*}$ (Where $\frac{dv(f_1)}{du}|_{E_{SN}^*}$ and $\frac{dv(f_2)}{du}|_{E_{SN}^*}$ denote the slope of $f_1(u, v) = 0$ and $f_2(u, v) = 0$ respectively at E_{SN}^*), since $\frac{dv(f_1)}{du}|_{E_{SN}^*} = \frac{\partial F_1/\partial u}{\partial F_1/\partial v}|_{E_{SN}^*}$ and $\frac{dv(f_2)}{du}|_{E_{SN}^*} = \frac{\partial F_2/\partial u}{\partial F_2/\partial v}|_{E_{SN}^*}$. Therefore $\det J_{E_{SN}^*} = 0$. Hence one of the eigenvalue of $J_{E_{SN}^*}$ is zero with multiplicity one. Now we check the transversality conditions for saddle-node bifurcation [29]. Let V and W be the eigenvectors of $J_{E_{SN}^*}$ and $[J_{E_{SN}^*}]^T$ corresponding to zero eigenvalue respectively.

First transversality condition for saddle node bifurcation

$$W^T F_E(E_{SN}^*; E_{SN}) = -v_{sn*}^2 \frac{a_{12}(u_{sn*}, v_{sn*})T_{11}(u_{sn*}, v_{sn*})}{a_{22}(u_{sn*}, v_{sn*})(D + 2E_{SN}v_{sn*})}.$$

Second transversality condition

$$W^T D^2 F(E_{SN}^*; E_{SN})(V, V) = I_0 + \frac{T_{11}Sv_{sn*}}{a_{22}(u_{sn*}, v_{sn*})} \cdot \left[\left(\frac{T_{11}(u_{sn*}, v_{sn*})}{D + 2E_{SN}v_{sn*}} \right) u_{sn*} - v_{sn*} \right]^2 - \frac{2E_{SN}a_{12}(u_{sn*}, v_{sn*})}{a_{22}(u_{sn*}, v_{sn*})} \left(\frac{T_{11}(u_{sn*}, v_{sn*})}{D + 2E_{SN}v_{sn*}} \right)^3.$$

Detail calculation is given in ‘‘Appendix 1’’. Since it is not possible to find out the explicit expression of $E_{SN}^*(u_{sn*}, v_{sn*})$ analytically, we check the occurrence of saddle-node bifurcation through a numerical example. Here we verify the saddle node bifurcation for the choice of parameters value. For the parameters value $A = 0.3$, $B = 0.15$, $C = 0.01$, $D = 0.1$ and $E = 0.2$ system (3)–(4) has two interior equilibrium points $E_{2*}(0.5678, 1.5726)$, $E_{1*}(0.8281, 1.7449)$. We decrease the parameter E and at threshold value $E_{SN} = 0.019004518564213$ two interior equilibrium coincides i.e. $E_{1*}(u_{sn*}, u_{sn*}) = E_{2*}(u_{sn*}, v_{sn*}) = (0.696801, 2.019398)$. Further decreasing the parameter E system has no interior equilibrium points. First transversality condition $W^T F_E(E_{SN}^*; E_{SN}) = -7.9713(\neq 0)$ and second transversality condition $W^T D^2 F(E_{SN}^*; E_{SN})(V, V) = -5.4217(\neq 0)$. We also get $\det((u_{sn*}, v_{sn*}))|_{E_{SN}} = 0$.

Ecologically, this bifurcation results the extinction for both the species as in this case origin is the only stable equilibrium point. Coexistence of both the species is observed for low conversion rate and the extinction occurs when the conversion rate is very high.

4.2 Hopf bifurcation

We note that E_{2*} is always a saddle point when it exists and stability of E_{1*} can change through Hopf-bifurcation, stated in the following theorem

Theorem 4.1 *Stability of E_{1*} gets changed through Hopf-bifurcation at the threshold $B = B_H = \frac{(u_{1*}^2 + Cv_{1*}^2)^2}{u_{1*}(u_{1*}^3 - Cu_{1*}v_{1*}^2 - 2Cv_{1*}^3)}$ ($T_{11}(u_{1*}, v_{1*}) - D - 2Ev_{1*}$) if $u_{1*} \neq 0$ and $u_{1*}^3 \neq Cv_{1*}^2(u_{1*} - 2v_{1*})$.*

Proof For $B = B_H$ clearly $\text{Tr}J(u_{1*}, v_{1*}) = 0$. Jacobian matrix evaluated at equilibrium point E_{1*} has a pair of purely imaginary eigenvalues. Now we check the transversality condition $\frac{d}{dB}\{Re(\lambda)\}|_{B=B_H} \neq 0$, where λ is an eigenvalue of the Jacobian matrix $J(u_{2*}, v_{2*})$ evaluated at $B = B_H$.

Eigenvalue for the Jacobian matrix is given by

$$\lambda = \frac{\text{Tr}J(u_{1*}, v_{1*}) \pm \sqrt{\text{Tr}^2 J(u_{1*}, v_{1*}) - 4 \det J(u_{1*}, v_{1*})}}{2}$$

Using the condition for Hopf-bifurcation i.e., $\text{tr}J_{E_{1*}}(u_{1*}, v_{1*}) = 0$, we get

$$\lambda = \pm \sqrt{-\det J(u_{1*}, v_{1*})}$$

From above λ is imaginary if $\det J(u_{1*}, v_{1*}) > 0$ and λ is real if $\det J(u_{1*}, v_{1*}) < 0$. Now taking λ is real and we calculate the expression as following

$$\begin{aligned} \frac{d}{dB}\{Re(\lambda)\}|_{B=B_H} &= \frac{d}{dB}\left[\sqrt{\det J(u_{1*}, v_{1*})}\right] \\ &= \frac{1}{2} \frac{\frac{d}{dB}\left[T_{11}(u_{1*}, v_{1*})a_{12}(u_{1*}, v_{1*}) - (T_{11}(u_{1*}, v_{1*}) - a_{22}(u_{1*}, v_{1*}))(D + 2Ev_{1*})\right]}{\sqrt{(T_{11}(u_{1*}, v_{1*})a_{12}(u_{1*}, v_{1*}) - (T_{11}(u_{1*}, v_{1*}) - a_{22}(u_{1*}, v_{1*}))(D + 2Ev_{1*}))}} \end{aligned}$$

$$\begin{aligned}
 &= \frac{T_{11}(u_{1*}, v_{1*})u_{1*}^2(u_{1*}^2 - Cv_{1*}^2) + 2Cu_{1*}v_{1*}^3(D + 2Ev_{1*})}{2(u_{1*}^2 + Cv_{1*}^2)^2 \sqrt{(T_{11}(u_{1*}, v_{1*})a_{12}(u_{1*}, v_{1*}) - (T_{11}(u_{1*}, v_{1*}) - a_{22}(u_{1*}, v_{1*}))(D + 2Ev_{1*}))}}, \\
 &= \sqrt{\frac{2Cu_{1*}v_{1*}^3 - u_{1*}^2(u_{1*}^2 - Cv_{1*}^2)}{T_{11}^2(u_{1*}, v_{1*})u_{1*}^2(u_{1*}^2 - Cv_{1*}^2) - 2Cu_{1*}v_{1*}^3(D + 2Ev_{1*})^2}} \left[\frac{T_{11}(u_{1*}, v_{1*})u_{1*}^2(u_{1*}^2 - Cv_{1*}^2) + 2Cu_{1*}v_{1*}^3(D + 2Ev_{1*})}{2(u_{1*}^2 + Cv_{1*}^2)^2} \right].
 \end{aligned}$$

Which is clearly non-zero using the conditions given in the statement of the theorem. □

We determine the stability of Hopf-bifurcating limit cycle by finding the first lyapunov number. To do so we translate the equilibrium point $E_{1*}(u_{1*}, v_{1*})$ to origin with new coordinate by setting $x = u - u_{1*}$, $y = v - v_{1*}$ and we get first lyapunov number l_1 . If $l_1 > 0$ then Hopf-bifurcating limit cycle is unstable and the corresponding Hopf-bifurcation is called subcritical. If $l_1 < 0$ then the Hopf-bifurcating limit cycle is stable and the Hopf-bifurcation is called supercritical. Detail calculation is given in “Appendix 2”.

Here we verify the hopf-bifurcation condition for the choice of parameters value numerically. We fixed the parameters value at $A = 0.3$, $C = 0.01$, $D = 0.1$, $E = 0.019$ and threshold value of $B_H = 0.1499372509$. We found the first Lyapunov coefficient is $7.109 > 0$, so the system undergoes a subcritical Hopf-bifurcation. This set of parameters value are satisfied the Hopf bifurcation condition mentioned in theorem (4.1) i.e. $u_{1*}^3 - Cv_{1*}^2(u_{1*} - 2v_{1*}) = 0.15948 (\neq 0)$ and satisfy the transversality condition $\frac{d}{dB} \{Re(\lambda)\}|_{B=B_H} = 0.14994 (\neq 0)$. Also we get $TrJ(u_{1*}, v_{1*})_{B_H} = 0$ and $\det J(u_{1*}, v_{1*})_{B_H} = 0.0035$ is positive.

Ecologically, unstable limit cycle arising through subcritical Hopf-bifurcation is the boundary of the basin of attraction of the stable equilibrium point. That is, the unstable limit cycle acts as a separatrix between the domain of attraction of coexistence state and extinction state of both populations. On the other hand, the presence of stable limit cycle through supercritical Hopf-bifurcation indicates that both the prey and predator populations have oscillatory coexistence.

4.3 Bogdanov-Takens bifurcation

Now saddle-node curve and Hopf-curve meet at Bogdanov-Takens bifurcation point. In this subsection, we show that the system (3)–(4) undergoes a Bogdanov-Takens bifurcation of co-dimension two. For this bifurcation, the Jacobian matrix evaluated at $E_{SN} = (u_{sn*}, v_{sn*})$ has a zero eigenvalue with algebraic multiplicity two. The parametric condition for this is given by $\det(J(u, v))|_{(E_{SN}^*; B_{BT}; E_{BT})} = 0$ and $Tr(J(u, v))|_{(E_{SN}^*; B_{BT}; E_{BT})} = 0$, where (B_{BT}, E_{BT}) is the B-T bifurcation point. Hence we find the expression for $E = E_{BT}$ and $B = B_{BT}$ as follow

$$E_{BT} = \frac{T_{11}(u_{sn*}, v_{sn*})(a_{12}(u_{sn*}, v_{sn*}) - D) + Da_{22}(u_{sn*}, v_{sn*})}{2v_{sn*}(T_{11}(u_{sn*}, v_{sn*}) - a_{22}(u_{sn*}, v_{sn*}))}$$

$$B_{BT} = \frac{(u_{sn*}^2 + Cv_{sn*}^2)^2}{u_{sn*}(u_{sn*}^3 - Cu_{sn*}v_{sn*}^2 - 2Cv_{sn*}^3)} (T_{11}(u_{sn*}, v_{sn*}) - D - 2E_{BT}v_{sn*}). \tag{7}$$

we have to check the transversality conditions for Bogdanov-Takens bifurcation and for this we consider the neighbourhood of BT point and a perturbation to the parameters B and E around their BT-bifurcation threshold given by $(B, E) \rightarrow (B_{BT} + \lambda_1, E_{BT} + \lambda_2)$, where $|\lambda_1|, |\lambda_2| \ll 1$. Therefore the system (3)–(4) become

$$\begin{aligned} \frac{du}{dT} &= u(1 - u) \left(\frac{u}{A} - 1 \right) - \frac{(B_{BT} + \lambda_1)u^2v}{u^2 + Cv^2} \equiv F_0^1(u, v) \\ \frac{dv}{dT} &= \frac{(B_{BT} + \lambda_1)u^2v}{u^2 + Cv^2} - Dv - (E_{BT} + \lambda_2)v^2 \equiv F_0^2(u, v) \end{aligned} \tag{8}$$

We transform the equilibrium point E_{SN}^* to origin by $x = u - u_{sn*}, y = v - v_{sn*}$ and we check the condition of nondegeneracy. Detail calculation is given in ‘‘Appendix 3’’.

Here we verify the Bogdanov-Takens bifurcation conditions for the choice of parameters value numerically. We choose parameters value $A = 0.3, C = 0.01, D = 0.11$ and threshold value of $B_{BT} = 0.2925, E_{BT} = 0.092825707, E(u_{sn*}, v_{sn*}) = (0.7177925570, 0.7177925570)$ satisfy the non degeneracy condition describe in ‘‘Appendix 3’’. We check the value of the expression $\eta_{20}(0) = 2.9146(\neq 0)$ and $\xi_{20}(0) + \eta_{11}(0) = -4.6983(\neq 0)$. Also $\text{Tr}J(u_{sn*}, v_{sn*})_{(E_{BT}, B_{BT})} = 0$ and $\det J(u_{sn*}, v_{sn*})_{(E_{BT}, B_{BT})} = 0$.

5 Global dynamical properties

In Sect. (4), we have described some local bifurcations under various parametric restrictions associated with the system (3)–(4). We observed that parameters B and E have important significance in the study of bifurcation theory for considered model. Here we plot a parametric bifurcation diagram in $B - E$ plane to determine how bifurcation curves breaks the positive quadrant of whole $B - E$ plane into different subregions and the system (3)–(4) experiences qualitatively different dynamic behavior in different subregions. System (3)–(4) exhibits local bifurcations (saddle node bifurcation, Hopf bifurcation and $B - T$ bifurcation) and global bifurcation (homoclinic). The occurrence of homoclinic bifurcation indicates that the stable limit cycle disappears. The whole $B - E$ plane is divided into five different subregions $R1, R2, R3, R4$ and $R5$ by local and global bifurcation curves. Schematic bifurcation diagram corresponding to the system (3)–(4) is presented in Fig. 3. System (3)–(4) has no interior equilibrium point when $(B, E) \in R1$. Below the BT point, we decrease the magnitude of parameter B in such a way that (B, E) enters into the region $R2$ and the system exhibits two interior equilibrium points. At threshold value E_{SN} where two interior equilibrium point emerges, a saddle node bifurcation appears and the saddle node bifurcation curve is represented by blue colour curve in Fig. 3. At the threshold value $B = B_H$, Hopf bifurcation occurs and the Hopf-bifurcation curve is represented

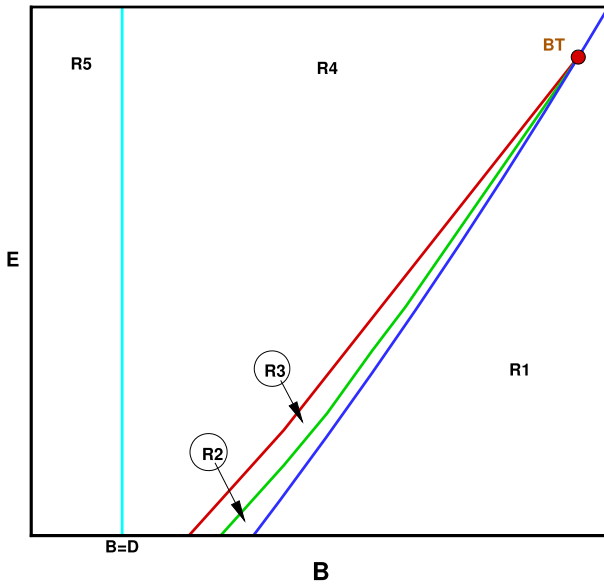


Fig. 3 Two parametric bifurcation diagram in $B - E$ plane

by green colour curve in Fig. 3. Then we reach at the region $R3$ after crossing the Hopf-bifurcation curve. Hopf-bifurcation curve and saddle node bifurcation curve meet at the point BT , where BT is the Bogdanov-Takens bifurcation point. Again crossing the homoclinic bifurcation curve we enter into the region $R4$, the homoclinic bifurcation curve emerges from BT point, represented by the red colour curve in Fig. 3. Further decreasing the value of parameter B under the restriction $B < D$ we reach at the region $R5$, where the system admits no interior equilibrium point.

Now we discuss the phase portraits for a particular choice of parameter set given by A, C, D and varying B and E to understand the stability and bifurcation analysis very well. We fixed the parameters values $A = 0.3, C = 0.01, D = 0.11$. Values of B and E will be chosen in such a way that the point (B, E) belongs to each of the five different domains presented in the schematic bifurcation diagram Fig. 3. Phase portraits corresponding to each domain are presented in Fig. 4. Different parameter values for B and E for different domains are given in the caption of the Fig. 4. In all the phase portraits, stable equilibrium points are marked with red dotted circle, saddle equilibrium points are marked with black open circle and unstable equilibrium points are marked with green dotted circle. In region $R1$, system (3)–(4) has no interior equilibrium point and equilibrium point E_0 is attractor, E_1, E_2 are repeller and saddle points, respectively. Hence $E_0 = (0, 0)$ is globally asymptotically stable here and all the trajectories starting from any initial condition will be attracted towards the origin which is evident from Fig. 4a. In domain $R2$, two interior equilibrium points $E_{1*}(u_{1*}, v_{1*})$ and $E_{2*}(u_{2*}, v_{2*})$ exist. $E_{2*}(u_{2*}, v_{2*})$ is saddle and $E_{1*}(u_{1*}, v_{1*})$ is unstable. Boundary equilibrium points have same nature like $R1$. The stable manifold of saddle equilibrium is shown by red colour curve in Fig. 4b. In domain $R3$, the

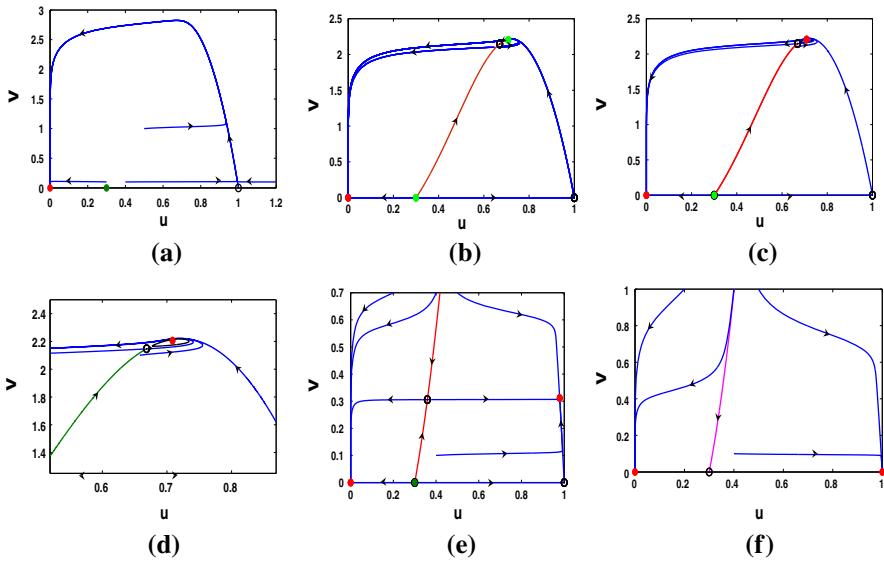


Fig. 4 Phase portraits for fixed parameter value $A = 0.3, C = 0.01, D = 0.11$ and varying B and E . **a** $B = 0.118, E = 0.0001$ chosen from region $R1$, **b** $B = 0.14, E = 0.01255$ chosen from region $R2$, **c** $B = 0.13984, E = 0.01462$ chosen from region $R3$, **d** enlarge version of **c**, **e** $B = 0.15, E = 0.16$ chosen from region $R4$, **f** $B = 0.1, E = 0.16$ chosen from region $R5$

unstable interior equilibrium point changes its stability through Hopf-bifurcation and it is surrounded by an unstable limit cycle. Trajectories starting from the inside of limit cycle will converge to the stable equilibrium, otherwise converge to the origin. Hence, unstable limit cycle acts as a separatrix in domain $R3$ (See Fig. 4c). Larger version of limit cycle is shown in Fig. 4d. We reach in the domain $R4$ through homoclinic bifurcation. Here, two interior equilibrium points exist. One is stable and another is the saddle. Boundary equilibrium points exist and they have the same stability properties like domain $R1, R2$ and $R3$. The red coloured curve acts as a separatrix between the domain of attraction of origin and stable interior equilibrium point i.e the trajectories starting right side of the separatrix will be attracted towards the stable interior equilibrium and trajectories starting left side of the separatrix will be attracted towards the origin (See Fig. 4e). In this domain stable coexistence of both populations is possible. In the domain $R5$, no interior equilibrium point exists. Equilibrium points E_0 and E_2 are attractor and equilibrium point E_1 is a saddle point. The stable manifold of E_1 is the separatrix between the domain of attraction of E_0 and E_2 which is evident from Fig. 4f.

5.1 Impact of Allee parameter in dynamics of system (3)–(4)

We have considered conversion rate of prey and death rate of predator as bifurcation parameters and have plotted the two parametric bifurcation diagram in $B - E$ plane in Fig. 3 to determine all possible bifurcations. Now we are interested to check the role

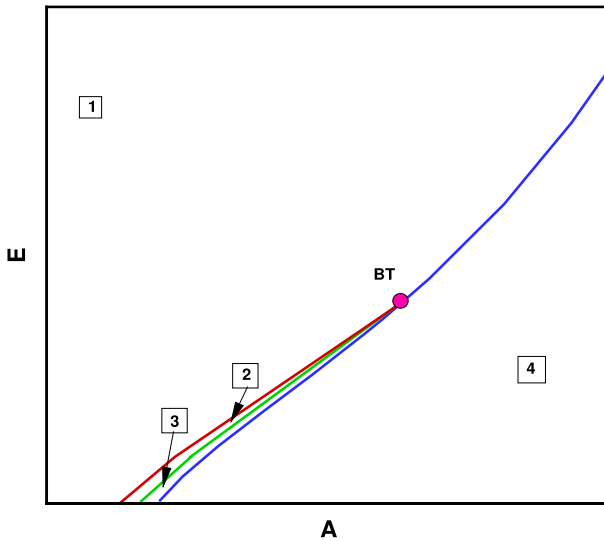


Fig. 5 Two parametric bifurcation diagram in $A - E$ plane. BT is the Bogdanov-Takens bifurcation point

Table 1 Equilibrium points and their stability for several domain of Fig. 3

Region	Interior equilibrium points	Nature of the phase portrait
R_1	Nil	E_0 is locally asymptotically stable, equilibrium point E_1 is unstable and equilibrium point E_2 is saddle
R_2	E_{1*}, E_{2*} exist	E_{2*} is saddle and E_{1*} is unstable, E_0 is locally asymptotically stable, equilibrium point E_1 is unstable and equilibrium point E_2 is saddle
R_3	E_{1*}, E_{2*} exist	E_{2*} is saddle and E_{1*} is stable bounded by unstable limit cycle and E_0 is locally asymptotically stable equilibrium point E_1 is unstable and equilibrium point E_2 is saddle
R_4	E_{1*}, E_{2*} exist	E_{2*} is saddle and E_{1*} is stable, E_0 is locally asymptotically stable, equilibrium point E_1 is unstable and equilibrium point E_2 is saddle
R_5	Nil	E_0 is locally asymptotically stable, equilibrium point E_1 is saddle and equilibrium point E_2 is stable

of Allee parameter in the dynamics of the system (3)–(4). We consider Allee effect parameter as one of bifurcation parameter, another one is density dependent death rate and plot two parametric bifurcation diagram in $A - E$ plane in Fig. 5. There are similarities in Figs. 3 and 5. Several bifurcation curves breaks the positive quadrant of whole $A - E$ plane into four different sub regions. Saddle node bifurcation curve is represented by blue coloured curve, hopf-bifurcation curve is represented by green coloured curve and red coloured curve is the homoclinic bifurcation curve in Fig. 5. Existence and stability of equilibrium points are same as Fig. 3 (Table 1).

6 System without Allee effect

Here we investigate the system (3)–(4) without Allee effect,

$$\frac{du}{dT} = u(1 - u) - \frac{Bu^2v}{u^2 + Cv^2}, \tag{9}$$

$$\frac{dv}{dT} = \frac{Bu^2v}{u^2 + Cv^2} - Dv - Ev^2, \tag{10}$$

where the biological meanings of the parameters are same as above. The model has the following two boundary equilibrium points: $E_{0na}(0, 0)$ and $E_{1na}(1, 0)$. The interior equilibrium points are the non-trivial intersection points of two nullclines (9) and (10) and the number of interior equilibria can be zero, one, two or three. Fig. 6 shows the possible number of interior equilibrium points for a particular set of parameters. We denote interior equilibrium point by $E_{ina}^*(u_{ina}^*, v_{ina}^*)$ ($i = 1, 2, 3$) and we assume the u -components of the interior equilibria satisfy the ordering $0 < u_{1na}^* < u_{2na}^* < u_{3na}^* < 1$ whenever they exist.

Here we plot a parametric bifurcation diagram in $B - E$ plane (see Fig. 7). The system (9)–(10) experiences qualitatively different dynamic behavior in different sub-regions. The eigenvalues of the Jacobian matrix of the system (9)–(10) at $E_{1na}(1, 0)$ are -1 and $B - D$. At $B = D$, $E_{1na}(1, 0)$ changes its stability and a transcritical bifurcation occurs. Ecologically, when conversion rate is equal to density independent death rate of predator, one coexistence state of both species is observed. When $B < D$, $E_{1na}(1, 0)$ is stable otherwise it is unstable. Stability analysis of $E_{0na}(0, 0)$ is described in ‘‘Appendix 4’’. Among three interior equilibrium points, E_{2na}^* is always saddle point and others two can change their stability through Hopf-bifurcation. We can check it numerically through Table 2.

Figure 7 shows that one Hopf-bifurcation curve, two saddle-node bifurcation curves, two transcritical bifurcation curves and one Homoclinic bifurcation curve divide first quadrant of $B - E$ plane into 9 subregions. Two Bogdanov-Takens bifurcation points

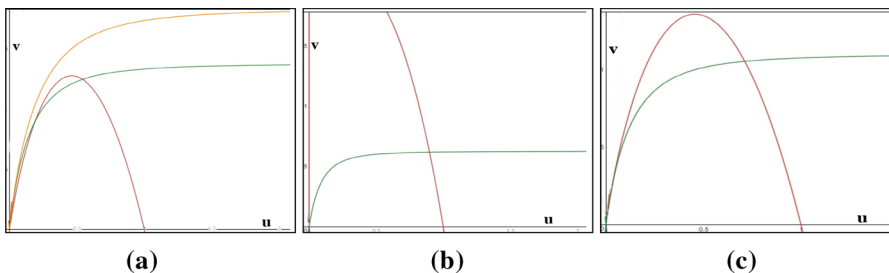


Fig. 6 Possible number of interior equilibrium points changes from zero to three for different values of B and E and other parameters are fixed at $C = 0.01, D = 0.1$. Red coloured curve is the first nullcline and green and orange coloured curved are second nullcline. **a** Interior equilibrium points change from zero to two through saddle-node bifurcation. $B = 0.21, E = 0.06$ (orange coloured, no interior equilibrium) and $B = 0.21, E = 0.08$ (green coloured, two interior equilibrium), **b** One interior equilibrium point for $B = 0.15, E = 0.08$ **c** Three interior equilibrium points for $B = 0.199, E = 0.09$

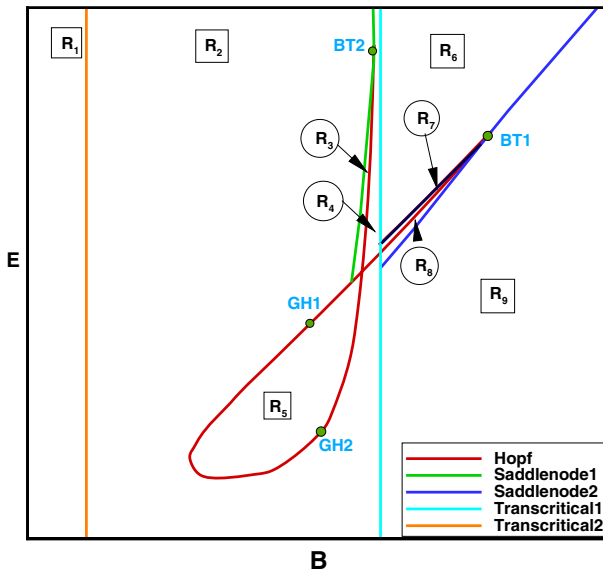


Fig. 7 Two parametric bifurcation diagram in $B - E$ plane of the system (9)–(10)

Table 2 Stability of the interior equilibrium points for fixed parameter $C = 0.01, D = 0.1$

Interior points	equilibrium	Parameter value	Eigenvalues	Stability
E_{1na}^*		$B = 0.199$	$\lambda_1 = -0.733763880850527e - 2$	Stable
		$E=0.06$	$\lambda_2 = -0.629988805914947e - 1$	
E_{1na}^*		$B = 0.197$	$\lambda_1 = 0.74487494e - 2 +$ $0.285267549264942e - 1 * I$	Unstable
		$E=0.06$	$\lambda_2 = 0.74487494e - 2 -$ $0.285267549264942e - 1 * I$	
E_{3na}^*		$B = 0.215$	$\lambda_1 = -0.3906688135e - 1 +$ $0.802523725240669e - 1 * I$	Stable
		$E=0.08$	$\lambda_2 = -0.3906688135e - 1 -$ $0.802523725240669e - 1 * I$	
E_{3na}^*		$B = 0.215$	$\lambda_1 = 0.4559824e - 3 +$ $0.325372491832114e - 1 * I$	Unstable
		$E=0.079$	$\lambda_2 = 0.4559824e - 3 -$ $0.325372491832114e - 1 * I$	
E_{2na}^*		$B = 0.215$	$\lambda_1 = 0.0471295768889850$	Saddle
		$E=0.079$	$\lambda_2 = -0.217552473889850e - 1$	

and two Bautin bifurcation points are also exist in the diagram. Corresponding phase portraits are shown in Fig. 8. Two vertical lines, orange coloured curve and cyan blue coloured curve are two transcritical bifurcation curves. Red coloured curve is the Hopf-bifurcation curve and black coloured curve is the homoclinic bifurcation curve.

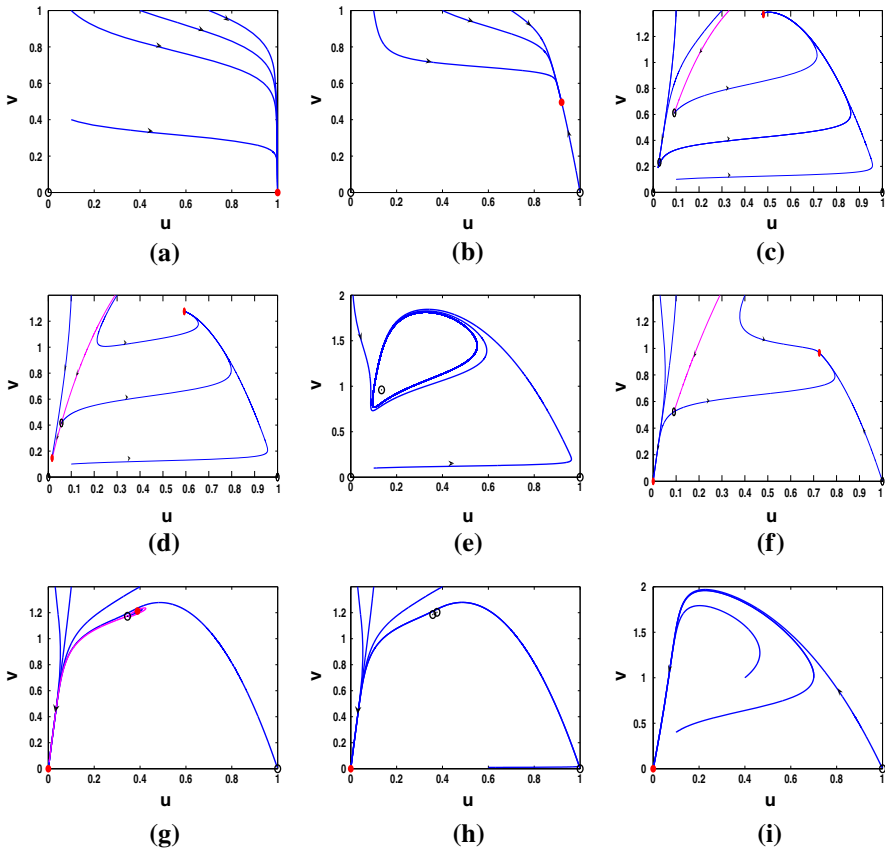


Fig. 8 Phase portrait for fixed $C = 0.01$, $D = 0.1$ and varying B and E . **a** $B = 0.01$, $E = 0.01$ (domain R_1); **b** $B = 0.15$, $E = 0.1$ (domain R_2); **c** $B = 0.197$, $E = 0.06$ (domain R_3); **d** $B = 0.198$, $E = 0.07$ (domain R_4); **e** $B = 0.183$, $E = 0.022$ (domain R_5); **f** $B = 0.21$, $E = 0.11$ (domain R_6); **g** $B = 0.215$, $E = 0.0791$ (domain R_7); **h** $B = 0.215$, $E = 0.079$ (domain R_8); **i** $B = 0.21$, $E = 0.01$ (domain R_9)

Two saddle node bifurcation curves are green and blue coloured curves. In domain R_1 , E_{1na} is the global stable point and no interior equilibrium points exist (see Fig. 8a). In domain R_2 , E_{1na} changes its stability and one stable interior equilibrium point E_{3na}^* appears through transcritical bifurcation (see Fig. 8b). E_{1na}^* and E_{2na}^* appear through saddle-node bifurcation in domain R_3 and E_{1na}^* is unstable in this domain and boundary equilibrium points have same nature like R_2 (see Fig. 8c). E_{1na}^* changes its stability through Hopf-bifurcation and become stable in domain R_4 (see Fig. 8d). In R_5 , E_{3na}^* exists and no equilibrium points are stable (see Fig. 8e). Interior equilibrium point E_{1na}^* disappears through another transcritical bifurcation and E_{3na}^* , E_{0na} are stable in domain R_6 (see Fig. 8f). In domain R_7 , E_{3na}^* is stable surrounded by an unstable limit cycle and boundary equilibrium points have same nature like R_6 (see Fig. 8g). E_{3na}^* changes its stability through another Hopf-bifurcation and become unstable in domain R_8 (see Fig. 8h). Interior equilibrium points E_{2na}^* and E_{3na}^* disappear through

another saddle-node bifurcation and E_{Ona} becomes globally stable equilibrium point in domain R_9 (see Fig. 8i). Existence and stability of the equilibrium points are summarized at Table 2. If we fixed parameters $C = 0.01$, $D = 0.1$, then the Bogdanov-Takens bifurcation (BT) points are $(B_{BT1}, E_{BT1}) = (0.21874235, 0.084215634)$ and $(B_{BT2}, E_{BT2}) = (0.19889577, 0.10111344)$. GH is the Bautin bifurcation point where first Lyapunov coefficient is zero and the threshold are $(B_{GH1}, E_{GH1}) = (0.18843566, 0.045024366)$ and $(B_{GH2}, E_{GH2}) = (0.18950869, 0.021593124)$.

6.1 Effect of density dependent predation rate

In this subsection, we present one parameter bifurcation diagram with respect to the density dependent predation rate to investigate the dynamical changes of our system (3)–(4) and (9)–(10). We vary the conversion rate B and fixed other parameters at $C = 0.01$, $D = 0.1$, $A = 0.3$ and (a), (b) $E = 0.025$; (c), (d) $E = 0.05$ (Fig. 9). Figure 9a,b for system (3)–(4) and Fig. 9c, d for system (9)–(10). In Fig. 9a and b, at most two interior equilibrium points exist on the right side of the black dotted vertical line $B = D$, one is stable and another one is unstable. Stable equilibrium point is represented by blue solid curve and unstable equilibrium point is represented by red dotted curve, two curves meet at a Hopf bifurcation point H . These two equilibrium points disappear through a saddle-node bifurcation point LP . In Fig. 9c and d, at most three interior equilibrium points exist. Stable equilibrium point is represented by blue solid curve and unstable equilibrium point is represented by red dotted curve. Axial equilibrium point $(1, 0)$ changes its stability through an orange coloured vertical transcritical bifurcation curve and one stable interior equilibrium point appears. Trivial equilibrium point $(0, 0)$ changes its stability through a cyan blue coloured vertical transcritical bifurcation curve and one interior equilibrium point disappears. The system undergoes two Hopf-bifurcations (denoted by ‘H’) and two saddle-node bifurcations (denoted by ‘LP’).

6.2 Comparison between Allee model and without Allee model

In this subsection, we have made the significant comparison of prey-predator model (3)–(4) with the model (9)–(10). In the model (3)–(4), we have considered strong Allee effect in prey growth but we have considered only logistic growth function for prey in the model (9)–(10). We observed that the Allee effect can simplify the dynamics of this type of prey-predator model. Comparing the dynamics of both the models we find the following differences:

1. System (3)–(4) has three axial equilibria and at most two interior equilibria whereas system (9)–(10) has two axial equilibria and at most three interior equilibria.
2. System (3)–(4) has axial equilibria $(0, 0)$, $(A, 0)$ and $(1, 0)$. $(0, 0)$ is always stable and $(1, 0)$ is stable when $B < D$. So it is possible that two axial equilibrium points are locally asymptotically stable at the same time when $B < D$. On the other hand system (9)–(10) has axial equilibria $(0, 0)$, $(1, 0)$. Both the axial equilibrium points change their stability through transcritical bifurcation and it is possible that no axial equilibrium point is stable in a certain time.

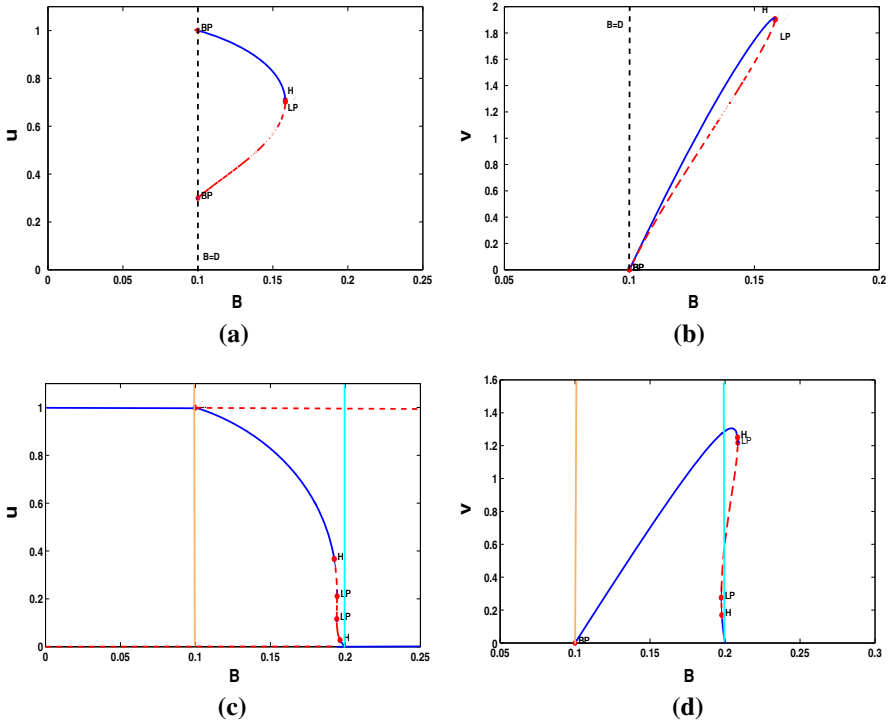


Fig. 9 One parameter bifurcation diagram in $B - u$ and $B - v$ plane represents the stability of equilibrium points. **a, b** for system (3)–(4) and **c, d** for system (9)–(10). Red Dotted line: unstable equilibria, blue solid line: stable equilibria, solid vertical line: transcritical bifurcation curves, LP : saddle-node bifurcation, H : Hopf bifurcation. Fixed parameters at $C = 0.01$, $D = 0.1$, $A = 0.3$ and **a, b** $E = 0.025$; **c, d** $E = 0.05$

3. System (3)–(4) has at most two interior equilibria, one is saddle and another one equilibrium point changes its stability through Hopf-bifurcation. The system (9)–(10) has at most three interior equilibrium points, one is saddle and two equilibrium points changes its stability through Hopf-bifurcation. Bistability is possible in this case, two interior equilibrium points are locally asymptotically stable in some regions (see Fig. 8d).
4. When conversion rate is very low, $(1, 0)$ is globally stable (see Fig. 8a) for the system (9)–(10) but in this case $(0, 0)$, $(1, 0)$ are both locally asymptotically stable (see Fig. 4f) for the system (3)–(4). When conversion rate is very high, origin is globally stable for both the systems.
5. No transcritical bifurcation occurs for the system (3)–(4) and one saddle-node bifurcation curve, one hopf-bifurcation curve, one homoclinic bifurcation curve meet at Bogdanov-Takens bifurcation point BT . The system (9)–(10) undergoes two transcritical bifurcations, two hopf-bifurcations, two saddle-node bifurcations and also homoclinic bifurcation. In this case we also get two Bogdanov-Takens bifurcation points.
6. In (3)–(4), Hopf-bifurcation is always subcritical. In (9)–(10), Hopf-bifurcation is subcritical as well as supercritical, we get two Bautin bifurcation points GH .

7 Discussion

In Allee effect model, coexistence state of prey and predator populations depends upon the conversion rate of prey and death rate of predator. When the conversion rate of prey is greater than the death rate of predator then coexistence state of both prey and predator populations is not possible. In this case, bistability occurs but the system goes to extinction for small initial prey density and stable state of prey is possible for large initial prey density. Origin is always an attractor and the basin of attraction of the origin depends upon the existence and stability of other equilibrium points. Both prey and predator populations in the system may coexist when the conversion rate of prey is less than the death rate of predator. It is quite difficult to find the explicit expressions for the coexistence state of prey and predator populations but detailed bifurcation analysis gives us the parametric restrictions to verify their existence and stability both. The summarized result are provided at Table 1. At most one of the interior equilibrium points is stable out of two interior equilibrium points. When the conversion rate of prey is very high then prey and predator populations do not coexist and the system goes to extinction for any prey density. From the phase portrait in Fig. 4, it is clear that the domain of attraction of attractor is depend upon the magnitude of model parameters. It is also observed that oscillatory coexistence is possible for both populations. Unstable limit cycle acts as boundary of attracting set of the stable interior equilibrium points. Local bifurcation curves in bifurcation diagram describe the change in the existence and stability properties of equilibrium points whereas global bifurcation curve shows considerable amount of effect in system dynamics. When the parameters enters from region R_3 to region R_4 (see Fig. 3) then homoclinic bifurcation occurs and basin of

Table 3 Equilibrium points and their stability for several domain of Fig. 7

Region	Interior equilibrium points	Nature of the phase portrait
R_1	Nil	E_{1na} is locally asymptotically stable and equilibrium point E_{0na} is saddle
R_2	E_{3na}^* exists	E_{0na}, E_{1na} are saddle and E_{3na}^* is locally asymptotically stable
R_3	$E_{1na}^*, E_{2na}^*, E_{3na}^*$ exist	$E_{0na}, E_{1na}, E_{2na}^*$ are saddle, E_{3na}^* is locally asymptotically stable and E_{1na}^* is unstable
R_4	$E_{1na}^*, E_{2na}^*, E_{3na}^*$ exist	E_{0na}, E_{1na} are saddle and E_{1na}^*, E_{3na}^* are locally asymptotically stable
R_5	E_{3na}^* exists	E_{0na}, E_{1na} are saddle and E_{3na}^* is unstable
R_6	E_{2na}^*, E_{3na}^* exist	E_{1na}, E_{2na}^* are saddle and E_{0na}, E_{3na}^* are locally asymptotically stable
R_7	E_{2na}^*, E_{3na}^* exist	E_{1na}, E_{2na}^* are saddle, E_{0na} is stable and E_{3na}^* is stable surrounded by an unstable limit cycle
R_8	E_{2na}^*, E_{3na}^* exist	E_{1na}, E_{2na}^* are saddle, E_{3na}^* is unstable and E_{0na} is locally asymptotically stable
R_9	Nil	E_{0na} is locally asymptotically stable and equilibrium point E_{1na} is saddle

attraction of E_{1*} changes significantly. The complete bifurcation analysis is described at global dynamics section.

The dynamics of the system is more complicated when Allee effect is not present in the system which is not common in prey-predator models studied before [27,38]. Origin is not always asymptotically stable point, which depends upon the conversion rate of prey. When conversion rate of prey is very high then origin is globally stable and it loose's its stability for low conversion rate of prey (see Figs. 10, 11). When conversion rate is very low, $(1, 0)$ is globally stable, i.e., predator can not survive but when conversion rate is equal to density independent death rate of predator, both the species can survive. The effect of conversion rate for both the species have been described in Sect. 6.1. We get more than one interior equilibrium points when density dependent death rate of predator is high and at most two of them are stable. Therefore, the stability of one interior equilibrium point is suppressed due to the Allee effect. It is also possible that no stable steady state for both the populations in the model without Allee effect (Fig. 8e). The summarized result of existence and stability of equilibrium points is provided at Table 3. All corresponding phase portraits are given in Fig. 8. With this comparison it is clear that Allee effect has a significant role in the dynamics of a prey-predator model with ratio dependent functional response and density dependent death rate of predator. Local extinction of populations in the prey-predator model can be preserved by the Allee effect. In the absence of Allee effect, stable limit cycle around unstable interior equilibrium point corresponding to the prey-predator model may occur. Comparison is given at Sect. 6.2.

Further generalization of this model can be studied in future. Environmental noise into the modelling approach is very important components for ecosystems, because parameters involved in the system always fluctuate in reality. In future, we can study the effect of environmental fluctuations in the given ecological model by extending the model into a stochastic differential equation model. Another important factor is time delay, which is a common nonlinearity. It is widely known that in reality time delays occur in almost every biological situation, so that we can not ignore them. It can stabilize or destabilize the coexistence steady-state. Hence, we can study the proposed prey-predator model with time delay also.

Acknowledgements Partha Sarathi Mandal and Koushik Garain's research are supported by SERB, DST project [grant: YSS/2015/001548]. Uday Kumar and Rakhi Sharma are supported by fellowship from MHRD, Government of India.

A Appendix 1

Transversality conditions for saddle-node bifurcation: Let V and W be the eigenvectors of $J_{E_{SN}^*}$ and $[J_{E_{SN}^*}]^T$ corresponding to zero eigenvalue respectively.

$$V = \begin{bmatrix} v_1 \\ v_2 \end{bmatrix}, \quad W = \begin{bmatrix} w_1 \\ w_2 \end{bmatrix}.$$

Then V should satisfy the following matrix equation

$$\begin{bmatrix} T_{11}(u_{sn*}, v_{sn*}) - a_{22}(u_{sn*}, v_{sn*}) & -a_{12}(u_{sn*}, v_{sn*}) \\ a_{22}(u_{sn*}, v_{sn*}) & a_{12}(u_{sn*}, v_{sn*}) - D - 2E_{SN}v_{sn*} \end{bmatrix} \begin{bmatrix} v_1 \\ v_2 \end{bmatrix} = \begin{bmatrix} 0 \\ 0 \end{bmatrix},$$

where $T_{11}(u_{sn*}, v_{sn*}) = (1 - u_{sn*})(\frac{u_{sn*}}{A} - 1) - u_{sn*}(\frac{u_{sn*}}{A} - 1) + \frac{u_{sn*}}{A}(1 - u_{sn*})$,
 $a_{12}(u_{sn*}, v_{sn*}) = \frac{Bu_{sn*}^2(u_{sn*}^2 - Cv_{sn*}^2)}{(u_{sn*}^2 + Cv_{sn*}^2)^2}$, $a_{22}(u_{sn*}, v_{sn*}) = \frac{2BCu_{sn*}v_{sn*}^3}{(u_{sn*}^2 + Cv_{sn*}^2)^2}$. Multiplying the second row by $T_{11} - a_{22}$, first row by a_{22} and subtracting the first row from above matrix, we get

$$\begin{bmatrix} T_{11}(u_{sn*}, v_{sn*}) - a_{22}(u_{sn*}, v_{sn*}) & -a_{12}(u_{sn*}, v_{sn*}) \\ 0 & (T_{11}(u_{sn*}, v_{sn*}) - a_{22}(u_{sn*}, v_{sn*}))(a_{12}(u_{sn*}, v_{sn*}) - D - 2E_{SN}v_{sn*}) \\ & + a_{12}(u_{sn*}, v_{sn*})a_{22}(u_{sn*}, v_{sn*}) \end{bmatrix} \begin{bmatrix} v_1 \\ v_2 \end{bmatrix} = \begin{bmatrix} 0 \\ 0 \end{bmatrix}.$$

To get the eigenvector the term $(T_{11}(u_{sn*}, v_{sn*}) - a_{22}(u_{sn*}, v_{sn*}))(a_{12}(u_{sn*}, v_{sn*}) - D - 2E_{SN}v_{sn*}) + a_{12}(u_{sn*}, v_{sn*})a_{22}(u_{sn*}, v_{sn*}) = 0$, which implies

$$(a_{12}(u_{sn*}, v_{sn*}) - D - 2E_{SN}v_{sn*}) = -\frac{a_{22}(D - 2E_{SN}v_{sn*})}{T_{11}(u_{sn*}, v_{sn*})} \tag{11}$$

and from above matrix equation, we have

$$a_{22}(u_{sn*}, v_{sn*})v_1 + (a_{12}(u_{sn*}, v_{sn*}) - D - 2E_{SN}v_{sn*})v_2 = 0. \tag{12}$$

Using Eqs. (11) and (12), we get

$$V = \left[1, \frac{T_{11}(u_{sn*}, v_{sn*})}{D + 2E_{SN}v_{sn*}} \right]^T.$$

Proceeding in a similar way the eigenvector of $[J_{E_{SN}^*}]^T$ is given by,

$$W = \left[-1, \frac{a_{12}(u_{sn*}, v_{sn*})T_{11}(u_{sn*}, v_{sn*})}{a_{22}(u_{sn*}, v_{sn*})(D + 2E_{SN}v_{sn*})} \right]^T$$

Let $F(u, v) = (F_1(u, v), F_2(u, v))^T$. Then $F_E(u, v) = (F_{1E}(u, v), F_{2E}(u, v))^T$. We can find from system (3)–(4), $F_{1E}|_{(E_{SN}^*; E_{SN})} = \frac{dF_1}{dE}|_{(E_{SN}^*; E_{SN})} = 0$ and $F_{2E}|_{(E_{SN}^*; E_{SN})} = \frac{dF_2}{dE}|_{(E_{SN}^*; E_{SN})} = -v_{sn*}^2$ and the first transversality condition for saddle node bifurcation becomes

$$\begin{aligned}
 W^T F_E(u, v) \Big|_{[E_{SN}^*; E_{SN}]} &= \left[-1 \frac{a_{12}(u_{SN^*}, v_{SN^*})T_{11}(u_{SN^*}, v_{SN^*})}{a_{22}(u_{SN^*}, v_{SN^*})(D+2E_{SN}v_{SN^*})} \right] \begin{bmatrix} 0 \\ -v_{SN^*}^2 \end{bmatrix} \\
 &= -v_{SN^*}^2 \frac{a_{12}(u_{SN^*}, v_{SN^*})T_{11}(u_{SN^*}, v_{SN^*})}{a_{22}(u_{SN^*}, v_{SN^*})(D+2E_{SN}v_{SN^*})}.
 \end{aligned}$$

Now for second transversality condition,

$$D^2 F(u, v)(V, V) = \sum_{i,j=1}^2 \frac{\partial^2 F(u, v)}{\partial u_i \partial u_j} v_i v_j, \text{ where } (u, v) = (u_1, u_2) \text{ (say)}. \text{ Then,}$$

$$\begin{aligned}
 D^2 \begin{pmatrix} F_1(u, v) \\ F_2(u, v) \end{pmatrix} (V, V) &= \begin{pmatrix} \sum_{i,j=1}^2 \frac{\partial^2 F_1(u, v)}{\partial u_i \partial u_j} v_i v_j \\ \sum_{i,j=1}^2 \frac{\partial^2 F_2(u, v)}{\partial u_i \partial u_j} v_i v_j \end{pmatrix} \\
 &= \begin{pmatrix} F_{1u_1^2} v_1^2 + 2F_{1u_1 u_2} v_1 v_2 + F_{1u_2^2} v_2^2 \\ F_{2u_1^2} v_1^2 + 2F_{2u_1 u_2} v_1 v_2 + F_{2u_2^2} v_2^2 \end{pmatrix},
 \end{aligned}$$

where $V = (v_1, v_2)^T$, $F_{1u_i u_j} = \frac{\partial^2 F_1}{\partial u_i \partial u_j}$ for $i, j = 1, 2$ and similarly for F_2 .

Using the equilibrium relation from Eq. (6), we get

$$\begin{aligned}
 D^2 F(E_{SN}^*; E_{SN})(V, V) &= \begin{pmatrix} I_0 - v_{SN^*}^3 S + 2S u_{SN^*} v_{SN^*}^2 \left(\frac{T_{11}(u_{SN^*}, v_{SN^*})}{D+2E_{SN}v_{SN^*}} \right) - S u_{SN^*}^2 v_{SN^*} \left(\frac{T_{11}(u_{SN^*}, v_{SN^*})}{D+2E_{SN}v_{SN^*}} \right)^2 \\ v_{SN^*}^3 S - 2S u_{SN^*} v_{SN^*}^2 \left(\frac{T_{11}(u_{SN^*}, v_{SN^*})}{D+2E_{SN}v_{SN^*}} \right) + (S u_{SN^*}^2 v_{SN^*} - 2E_{SN}) \left(\frac{T_{11}(u_{SN^*}, v_{SN^*})}{D+2E_{SN}v_{SN^*}} \right)^2 \end{pmatrix},
 \end{aligned}$$

where $I_0 = -\frac{6u_{SN^*}}{A} + \frac{2(1+A)}{A}$, $S = \frac{2BC(Cv_{SN^*}^2 - 3u_{SN^*}^2)}{(u_{SN^*}^2 + Cv_{SN^*}^2)^3}$. We find the expression

$$\begin{aligned}
 W^T D^2 F(E_{SN}^*; E_{SN})(V, V) &= I_0 + \frac{T_{11} S v_{SN^*}}{a_{22}(u_{SN^*}, v_{SN^*})} \cdot \left[\left(\frac{T_{11}(u_{SN^*}, v_{SN^*})}{D+2E_{SN}v_{SN^*}} \right) u_{SN^*} - v_{SN^*} \right]^2 \\
 &\quad - \frac{2E_{SN} a_{12}(u_{SN^*}, v_{SN^*})}{a_{22}(u_{SN^*}, v_{SN^*})} \left(\frac{T_{11}(u_{SN^*}, v_{SN^*})}{D+2E_{SN}v_{SN^*}} \right)^3.
 \end{aligned}$$

B Appendix 2

We calculate the first lyapunov number for stability of Hopf-bifurcation.

We translate the equilibrium point $E_{1^*}(u_{1^*}, v_{1^*})$ to origin with new coordinate By setting $x = u - u_{1^*}$, $y = v - v_{1^*}$. Then new system in coordinate (x, y) has power series expansion as given below

$$\begin{aligned}\dot{x} &= ax + by + (a_{20}x^2 + a_{11}xy + a_{02}y^2) + (a_{30}x^3 + a_{12}x^2y + a_{21}xy^2) \\ &\quad + Q_1(|x, y|^4), \\ \dot{y} &= cx + dy + (b_{20}x^2 + b_{11}xy + b_{02}y^2) + (b_{30}x^3 + b_{21}x^2y + b_{12}xy^2) \\ &\quad + Q_2(|x, y|^4).\end{aligned}$$

Where

$$\begin{aligned}a &= \left[\frac{\partial F_1(u, v)}{\partial u} \right] \Big|_{(E_{1*}; B_H)} = \frac{-3u_{1*}^2}{A} + 2u_{1*} \left(\frac{1}{A} + 1 \right) - 1 - \frac{2B_H C u_{1*} v_{1*}^3}{(u_{1*}^2 + C v_{1*}^2)^2}, \\ b &= \left[\frac{\partial F_1(u, v)}{\partial v} \right] \Big|_{(E_{1*}; B_H)} = -\frac{B_H u_{1*}^2 (u_{1*}^2 - C v_{1*}^2)}{(u_{1*}^2 + C v_{1*}^2)^2}, \\ c &= \left[\frac{\partial F_2(u, v)}{\partial u} \right] \Big|_{(E_{1*}; B_H)} = \frac{2B_H C u_{1*} v_{1*}^3}{(u_{1*}^2 + C v_{1*}^2)^2}, \\ d &= \left[\frac{\partial F_2(u, v)}{\partial v} \right] \Big|_{(E_{1*}; B_H)} = \frac{B_H u_{1*}^2 (u_{1*}^2 - C v_{1*}^2)}{(u_{1*}^2 + C v_{1*}^2)^2} - D - 2E v_{1*}, \\ a_{20} &= \frac{1}{2} \left[\frac{\partial^2 F_1(u, v)}{\partial u^2} \right] \Big|_{(E_{1*}; B_H)} = \frac{-3u_{1*}}{A} + \left(\frac{1}{A} + 1 \right) - \frac{B_H C v_{1*}^3 (C v_{1*}^2 - 3u_{1*}^2)}{(u_{1*}^2 + C v_{1*}^2)^3}, \\ a_{11} &= \left[\frac{\partial^2 F_1(u, v)}{\partial u \partial v} \right] \Big|_{(E_{1*}; B_H)} = \frac{2B_H C u_{1*} v_{1*}^2 (C v_{1*}^2 - 3u_{1*}^2)}{(u_{1*}^2 + C v_{1*}^2)^3}, \\ a_{02} &= \frac{1}{2} \left[\frac{\partial^2 F_1(u, v)}{\partial v^2} \right] \Big|_{(E_{1*}; B_H)} = \frac{-B_H C u_{1*}^2 v_{1*} (C v_{1*}^2 - 3u_{1*}^2)}{(u_{1*}^2 + C v_{1*}^2)^3}, \\ a_{30} &= \frac{1}{6} \left[\frac{\partial^3 F_1(u, v)}{\partial u^3} \right] \Big|_{(E_{1*}; B_H)} = -\frac{1}{A} - \frac{B_H C u_{1*} v_{1*}^3 (u_{1*}^2 - C v_{1*}^2)}{3(u_{1*}^2 + C v_{1*}^2)^4}, \\ a_{21} &= \frac{1}{2} \left[\frac{\partial^3 F_1(u, v)}{\partial u^2 \partial v} \right] \Big|_{(E_{1*}; B_H)} = -\frac{B_H C v_{1*}^2 (9u_{1*}^4 - 14C u_{1*}^2 v_{1*}^2 + C^2 v_{1*}^4)}{(u_{1*}^2 + C v_{1*}^2)^4}, \\ a_{12} &= \frac{1}{2} \left[\frac{\partial^3 F_1(u, v)}{\partial u \partial v^2} \right] \Big|_{(E_{1*}; B_H)} = \frac{B_H C v_{1*} (6u_{1*}^5 - 16C u_{1*}^3 v_{1*}^2 + 2C^2 u_{1*} v_{1*}^4)}{(u_{1*}^2 + C v_{1*}^2)^4}, \\ a_{03} &= \frac{1}{6} \left[\frac{\partial^3 F_1(u, v)}{\partial v^3} \right] \Big|_{(E_{1*}; B_H)} = \frac{-B_H C u_{1*}^2 (6C u_{1*}^2 v_{1*}^2 - C^2 v_{1*}^4 - u_{1*}^4)}{(u_{1*}^2 + C v_{1*}^2)^4}, \\ b_{20} &= \frac{1}{2} \left[\frac{\partial^2 F_2(u, v)}{\partial u^2} \right] \Big|_{(E_{1*}; B_H)} = \frac{B_H C v_{1*}^3 (C v_{1*}^2 - 3u_{1*}^2)}{(u_{1*}^2 + C v_{1*}^2)^3}, \\ b_{11} &= \left[\frac{\partial^2 F_2(u, v)}{\partial u \partial v} \right] \Big|_{(E_{1*}; B_H)} = \frac{-2B_H C u_{1*} v_{1*}^2 (C v_{1*}^2 - 3u_{1*}^2)}{(u_{1*}^2 + C v_{1*}^2)^3}, \\ b_{02} &= \frac{1}{2} \left[\frac{\partial^2 F_2(u, v)}{\partial v^2} \right] \Big|_{(E_{1*}; B_H)} = \frac{B_H C u_{1*}^2 v_{1*} (C v_{1*}^2 - 3u_{1*}^2)}{(u_{1*}^2 + C v_{1*}^2)^3} - E,\end{aligned}$$

$$\begin{aligned}
 b_{30} &= \frac{1}{6} \left[\frac{\partial^3 F_2(u, v)}{\partial u^3} \right] \Big|_{(E_{1*}; B_H)} = -\frac{1}{A} + \frac{4B_H C u_{1*} v_{1*}^3 (C v_{1*}^2 - u_{1*}^2)}{(u_{1*}^2 + C v_{1*}^2)^4}, \\
 b_{21} &= \frac{1}{2} \left[\frac{\partial^3 F_2(u, v)}{\partial u^2 \partial v} \right] \Big|_{(E_{1*}; B_H)} = -\frac{B_H C v_{1*}^2 (9u_{1*}^4 - 14C u_{1*}^2 v_{1*}^2 + C^2 v_{1*}^4)}{(u_{1*}^2 + C v_{1*}^2)^4}, \\
 b_{12} &= \frac{1}{2} \left[\frac{\partial^3 F_2(u, v)}{\partial u \partial v^2} \right] \Big|_{(E_{1*}; B_H)} = \frac{B_H C v_{1*} (6u_{1*}^5 - 16C u_{1*}^3 v_{1*}^2 + 2C^2 u_{1*} v_{1*}^4)}{(u_{1*}^2 + C v_{1*}^2)^4}, \\
 b_{03} &= \frac{1}{6} \left[\frac{\partial^3 F_2(u, v)}{\partial v^3} \right] \Big|_{(E_{1*}; B_H)} = \frac{B_H C u_{1*}^2 (6C u_{1*}^2 v_{1*} - C^2 v_{1*}^4 - u_{1*}^4)}{(u_{1*}^2 + C v_{1*}^2)^4}.
 \end{aligned}$$

We can calculate Lypunov first coefficient by using (13) as given below

$$\begin{aligned}
 l_1 &= \frac{-3\pi}{2bD_1^{\frac{3}{2}}} [ac(a_{11}^2 + a_{11}b_{02} + a_{02}b_{11}) + ab(b_{11}^2 + a_{20}b_{11} + a_{11}b_{02}) \\
 &\quad + c^2(a_{11}a_{02} + 2a_{02}b_{02}) \\
 &\quad - 2ac(b_{02}^2 - a_{20}a_{02}) - 2ab(a_{20}^2 - b_{20}b_{02}) - b^2(2a_{20}b_{20} + b_{11}b_{20}) + (bc - 2a^2) \\
 &\quad (b_{11}b_{02} - a_{11}a_{20}) - (a^2 + bc)\{3(cb_{03} - ba_{30}) + 2a(a_{21} + b_{12}) + (ca_{12} - bb_{21})\}],
 \end{aligned}$$

where $D_1 = ad - bc$. we get the expression for Lypunov first coefficient as:

$$l_1 = \frac{3\pi}{2bD_1^{\frac{3}{2}}} L.$$

where

$$\begin{aligned}
 L &= [ac(a_{11}^2 + a_{11}b_{02} + a_{02}b_{11}) + ab(b_{11}^2 + a_{20}b_{11} + a_{11}b_{02}) + c^2(a_{11}a_{02} + 2a_{02}b_{02}) \\
 &\quad - 2ac(b_{02}^2 - a_{20}a_{02}) - 2ab(a_{20}^2 - b_{20}b_{02}) - b^2(2a_{20}b_{20} + b_{11}b_{20}) + (bc - 2a^2) \\
 &\quad (b_{11}b_{02} - a_{11}a_{20}) - (a^2 + bc)\{3(cb_{03} - ba_{30}) + 2a(a_{21} + b_{12}) + (ca_{12} - bb_{21})\}].
 \end{aligned}$$

The limit cycle is unstable for $l_1 > 0$ and stable if $l_1 < 0$. Therefore, the Hopf-bifurcation is subcritical if $l_1 > 0$ and supercritical if $l_1 < 0$.

C Appendix 3

Transversality conditions for Bogdanov-Takens bifurcation : We transform the equilibrium point E_{SN}^* to origin by $x = u - u_{sn*}$, $y = v - v_{sn*}$ and we get

$$\begin{aligned}
 \dot{x}_1 &= a'x_1 + b'x_2 - \frac{2\lambda_1 C u_{sn*} v_{sn*}^3 x_1}{(u_{sn*}^2 + C v_{sn*}^2)^2} - \frac{\lambda_1 u_{sn*}^2 (u_{sn*}^2 - C v_{sn*}^2) x_2}{(u_{sn*}^2 + C v_{sn*}^2)^2} \\
 &\quad + \frac{p_{11}}{2} x_1^2 + p_{12} x_1 x_2 + \frac{p_{22}}{2} x_2^2 + \dots,
 \end{aligned}$$

$$\begin{aligned} \dot{x}_2 = & c'x_1 + d'x_2 + \frac{2\lambda_1Cu_{sn*}v_{sn*}^3x_1}{(u_{sn*}^2 + Cv_{sn*}^2)^2} + \left(\frac{\lambda_1u_{sn*}^2(u_{sn*}^2 - Cv_{sn*}^2)}{(u_{sn*}^2 + Cv_{sn*}^2)^2} - 2\lambda_2v_{sn*} \right) x_2 \\ & + \frac{q_{11}}{2}x_1^2 + q_{12}x_1x_2 + \frac{q_{22}}{2}x_2^2 + \dots, \end{aligned}$$

where a', b', c', d' are the element of the Jacobian matrix evaluated at an equilibrium point E_{SN}^* and $p_{11}, p_{12}, p_{22}, q_{11}, q_{12}, q_{22}$ are as follow

$$\begin{aligned} a' = & \left[\frac{\partial F_0^1(u, v)}{\partial u} \right]_{(E_{SN}^*; B_{BT}; E_{BT})} = \frac{-3u_{sn*}^2}{A} + 2u_{sn*} \left(\frac{1}{A} + 1 \right) \\ & - 1 - \frac{2B_{BT}Cu_{sn*}v_{sn*}^3}{(u_{sn*}^2 + Cv_{sn*}^2)^2}, \\ b' = & \left[\frac{\partial F_0^1(u, v)}{\partial v} \right]_{(E_{SN}^*; B_{BT}; E_{BT})} = -\frac{B_{BT}u_{sn*}^2(u_{sn*}^2 - Cv_{sn*}^2)}{(u_{sn*}^2 + Cv_{sn*}^2)^2}, \\ c' = & \left[\frac{\partial F_0^2(u, v)}{\partial u} \right]_{(E_{SN}^*; B_{BT}; E_{BT})} = \frac{2B_{BT}Cu_{sn*}v_{sn*}^3}{(u_{sn*}^2 + Cv_{sn*}^2)^2}, \\ d' = & \left[\frac{\partial F_0^2(u, v)}{\partial v} \right]_{(E_{SN}^*; B_{BT}; E_{BT})} = \frac{B_{BT}u_{sn*}^2(u_{sn*}^2 - Cv_{sn*}^2)}{(u_{sn*}^2 + Cv_{sn*}^2)^2} - D - 2E_{BT}v_{sn*}, \\ p_{11} = & \left[\frac{\partial^2 F_0^1(u, v)}{\partial u^2} \right]_{(E_{SN}^*; B_{BT}; E_{BT})} = \frac{-6u_{sn*}}{A} + 2 \left(\frac{1}{A} + 1 \right) \\ & - \frac{2B_{BT}Cv_{sn*}^3(Cv_{sn*}^2 - 3u_{sn*}^2)}{(u_{sn*}^2 + Cv_{sn*}^2)^3}, \\ p_{12} = & \left[\frac{\partial^2 F_0^1(u, v)}{\partial u \partial v} \right]_{(E_{SN}^*; B_{BT}; E_{BT})} = \frac{2B_{BT}Cu_{sn*}v_{sn*}^2(Cv_{sn*}^2 - 3u_{sn*}^2)}{(u_{sn*}^2 + Cv_{sn*}^2)^3}, \\ p_{22} = & \left[\frac{\partial^2 F_0^1(u, v)}{\partial v^2} \right]_{(E_{SN}^*; B_{BT}; E_{BT})} = \frac{-2B_{BT}Cu_{sn*}^2v_{sn*}(Cv_{sn*}^2 - 3u_{sn*}^2)}{(u_{sn*}^2 + Cv_{sn*}^2)^3}, \\ q_{11} = & \left[\frac{\partial^2 F_0^2(u, v)}{\partial u^2} \right]_{(E_{SN}^*; B_{BT}; E_{BT})} = \frac{2B_{BT}Cv_{sn*}^3(Cv_{sn*}^2 - 3u_{sn*}^2)}{(u_{sn*}^2 + Cv_{sn*}^2)^3}, \\ q_{12} = & \left[\frac{\partial^2 F_0^2(u, v)}{\partial u \partial v} \right]_{(E_{SN}^*; B_{BT}; E_{BT})} = \frac{-2B_{BT}Cu_{sn*}v_{sn*}^2(Cv_{sn*}^2 - 3u_{sn*}^2)}{(u_{sn*}^2 + Cv_{sn*}^2)^3}, \\ q_{22} = & \left[\frac{\partial^2 F_0^2(u, v)}{\partial v^2} \right]_{(E_{SN}^*; B_{BT}; E_{BT})} = \frac{2B_{BT}Cu_{sn*}^2v_{sn*}(Cv_{sn*}^2 - 3u_{sn*}^2)}{(u_{sn*}^2 + Cv_{sn*}^2)^3} - 2E_{BT}. \end{aligned}$$

Now we use affine transformation $y_1 = x, y_2 = a'x + b'y$ in (13) to get the new transformed system in (y_1, y_2) as:

$$\begin{aligned} \dot{y}_1 = & y_2 + \frac{u_{sn*}\lambda_1(a'u_{sn*}(u_{sn*}^2 - Cv_{sn*}^2) - 2b'Cv_{sn*}^3)}{b'(u_{sn*}^2 + Cv_{sn*}^2)}y_1 \\ & - \frac{u_{sn*}^2\lambda_1(u_{sn*}^2 - Cv_{sn*}^2)}{b'(u_{sn*}^2 + Cv_{sn*}^2)}y_2 + \left(\frac{p_{11}}{2} - \frac{a'p_{12}}{b'} \right) \end{aligned}$$

$$\begin{aligned}
& + \frac{a'^2 p_{22}}{2b'^2} y_1^2 + \left(\frac{p_{12}}{b'} - \frac{a' p_{22}}{b'^2} \right) y_1 y_2 + \frac{p_{22}}{2b'^2} y_2^2. \\
\dot{y}_2 = & (b'c' - a'd')y_1 + (a' + d')y_2 \\
& + \left(\frac{(a' - b')(a'\lambda_1 u_{sn*}^2 (u_{sn*}^2 - C v_{sn*}^2) - 2\lambda_1 b' C u_{sn*} v_{sn*}^3)}{b'(u_{sn*}^2 + C v_{sn*}^2)} \right. \\
& + 2a'\lambda_2 v_{sn*} \left. \right) y_1 - \left(2\lambda_2 v_{sn*} + \frac{(a' - b')\lambda_1 u_{sn*}^2 (u_{sn*}^2 - C v_{sn*}^2)}{b'(u_{sn*}^2 + C v_{sn*}^2)} \right) y_2 \\
& + \left(\frac{1}{b'} (a' p_{12} + b' q_{12}) \right. \\
& - \frac{a'}{b^2} (a' p_{22} + b' q_{22}) \left. \right) y_1 y_2 + \left(\frac{1}{2} (a' p_{11} + b' q_{11}) \right. \\
& - \frac{a'}{b'} (a' p_{12} + b' q_{12}) + \frac{a'^2}{2b'^2} (a' p_{22} \\
& \left. + b' q_{22}) \right) y_1^2 + \left(\frac{a' p_{22} + b' q_{22}}{2b'^2} \right) y_2^2.
\end{aligned}$$

which can be written as

$$\begin{aligned}
\dot{y}_1 = & y_2 + \xi_{00}(\lambda) + \xi_{10}(\lambda)y_1 + \xi_{01}(\lambda)y_2 + \frac{1}{2}\xi_{20}(\lambda)y_1^2 + \xi_{11}(\lambda)y_1 y_2 \\
& + \frac{1}{2}\xi_{02}(\lambda)y_2^2 + O_1(y_1 y_2). \\
\dot{y}_2 = & \eta_{00}(\lambda) + \eta_{10}(\lambda)y_1 + \eta_{01}(\lambda)y_2 + \frac{1}{2}\eta_{20}(\lambda)y_1^2 + \eta_{11}(\lambda)y_1 y_2 \\
& + \frac{1}{2}\eta_{02}(\lambda)y_2^2 + O_2(y_1 y_2).
\end{aligned}$$

where $\lambda = (\lambda_1, \lambda_2)$

$$\begin{aligned}
\xi_{00}(\lambda) = 0, \quad \xi_{10}(\lambda) &= \frac{u_{sn*} \lambda_1 (a' u_{sn*} (u_{sn*}^2 - C v_{sn*}^2) - 2b' C v_{sn*}^3)}{b'(u_{sn*}^2 + C v_{sn*}^2)}, \\
\xi_{01}(\lambda) &= \frac{-u_{sn*}^2 \lambda_1 (u_{sn*}^2 - C v_{sn*}^2)}{b'(u_{sn*}^2 + C v_{sn*}^2)} \\
\xi_{20}(\lambda) &= 2 \left(\frac{p_{11}}{2} - \frac{a' p_{12}}{b'} + \frac{a'^2 p_{22}}{2b'^2} \right), \quad \xi_{11}(\lambda) = \left(\frac{p_{12}}{b'} - \frac{a' p_{22}}{b'^2} \right), \\
\xi_{02}(\lambda) &= \frac{p_{22}}{b'^2}, \quad \eta_{00}(\lambda) = 0, \\
\eta_{10}(\lambda) &= (b'c' - a'd') \\
& + \left(\frac{(a' - b') \{ a'\lambda_1 u_{sn*}^2 (u_{sn*}^2 - C v_{sn*}^2) - 2\lambda_1 b' C u_{sn*} v_{sn*}^3 \}}{b'(u_{sn*}^2 + C v_{sn*}^2)} + 2a'\lambda_2 v_{sn*} \right)
\end{aligned}$$

$$\begin{aligned} \eta_{01}(\lambda) &= (a' + d') - \left(2\lambda_2 v_{sn*} + \frac{(a' - b')\lambda_1 u_{sn*}^2 (u_{sn*}^2 - C v_{sn*}^2)}{b'(u_{sn*}^2 + C v_{sn*}^2)} \right) \\ \eta_{20}(\lambda) &= 2\left(\frac{1}{2}(a' p_{11} + b' q_{11}) - \frac{a'}{b'}(a' p_{12} + b' q_{12}) + \frac{a'^2}{2b'^2}(a' p_{22} + b' q_{22}) \right) \\ \eta_{11}(\lambda) &= \left(\frac{1}{b'}(a' p_{12} + b' q_{12}) - \frac{a'}{b'^2}(a' p_{22} + b' q_{22}) \right), \eta_{02}(\lambda) = 2\left(\frac{a' p_{22} + b' q_{22}}{2b'^2} \right) \end{aligned}$$

Now

$$\begin{aligned} \xi_{20}(0) &= 2\left(\frac{p_{11}}{2} - \frac{a' p_{12}}{b'} + \frac{a'^2 p_{22}}{2b'^2} \right)_{\lambda=0}, \\ \eta_{11}(0) &= \left(\frac{1}{b'}(a' p_{12} + b' q_{12}) - \frac{a'}{b'^2}(a' p_{22} + b' q_{22}) \right)_{\lambda=0}, \\ \eta_{20}(0) &= 2\left(\frac{1}{2}(a' p_{11} + b' q_{11}) - \frac{a'}{b'}(a' p_{12} + b' q_{12}) + \frac{a'^2}{2b'^2}(a' p_{22} + b' q_{22}) \right)_{\lambda=0}. \end{aligned} \tag{13}$$

To check the non degeneracy conditions of Bogdanov-Takens bifurcation we have to check the following quantities:

$$(i) \begin{bmatrix} a' & b' \\ c' & d' \end{bmatrix} \neq 0_{2 \times 2}, \quad (ii) \xi_{20}(0) + \eta_{11}(0) \neq 0, \quad (iii) \eta_{20}(0) \neq 0.$$

The first condition is clearly satisfied. Also

$$\begin{aligned} \xi_{20}(0) + \eta_{11}(0) &= 2\left(\frac{p_{11}}{2} - \frac{a' p_{12}}{b'} + \frac{a'^2 p_{22}}{2b'^2} \right) \\ &\quad + \left(\frac{1}{b'}(a' p_{12} + b' q_{12}) - \frac{a'}{b'^2}(a' p_{22} + b' q_{22}) \right) \end{aligned}$$

D Appendix 4

Here we discuss the stability of the axial equilibrium point $E_0(0, 0)$ of the model (9)–(10). Now we transform the variables to new variables by replacing $p = \frac{v}{u}$ and we get the following system

$$\frac{du}{dT} = u(1 - u) - \frac{Bpu}{1 + Cp^2}, \tag{14}$$

$$\frac{dp}{dT} = \frac{Bp}{1 + Cp^2} + \frac{Bp^2}{1 + Cp^2} - Dp - Ep^2u - (1 - u)p. \tag{15}$$

We are interested here of the axial equilibrium points on the p -axis only. Axial equilibrium points on the p -axis are $(0, 0)$ and $(0, \mu_{1,2})$, where $\mu_{1,2}$ are the two roots of the quadratic equation

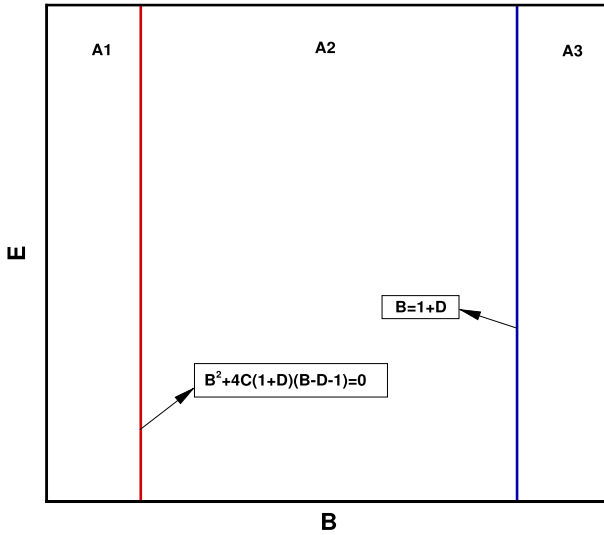


Fig. 10 Bifurcation diagram in $B - E$ plane of the axial equilibrium point $E_0(0, 0)$

$$\frac{B}{1 + Cp^2} + \frac{Bp}{1 + Cp^2} - D - 1 = 0$$

$$\Rightarrow p = \frac{B \pm \sqrt{B^2 + 4C(1 + D)(B - D - 1)}}{2C(1 + D)}$$

So $\mu_1 = \frac{B + \sqrt{B^2 + 4C(1 + D)(B - D - 1)}}{2C(1 + D)}$ and $\mu_2 = \frac{B - \sqrt{B^2 + 4C(1 + D)(B - D - 1)}}{2C(1 + D)}$. Eigenvalues of the Jacobian matrix evaluated at $(0, 0)$ is 1 and $B - (1 + D)$. Eigenvalues evaluated at $(0, \mu_{1,2})$ are $-\frac{B\mu_{1,2}}{1 + C\mu_{1,2}^2}$ and $-D - 1 + \frac{B(1 - C\mu_{1,2}^2 + 2\mu_{1,2})}{(1 + C\mu_{1,2}^2)^2}$. Now we discuss the different cases

- (i) If $(B - D - 1) < 0$ and $B^2 + 4C(1 + D)(B - D - 1) < 0$, then $(0, \mu_{1,2})$ do not exist and $(0, 0)$ is saddle point.
- (ii) If $(B - D - 1) < 0$ and $B^2 + 4C(1 + D)(B - D - 1) > 0$, then $(0, \mu_{1,2})$ exist. $(0, 0)$ is saddle point and $(0, \mu_{1,2})$ are stable points.
- (iii) If $(B - D - 1) > 0$ then $B^2 + 4C(1 + D)(B - D - 1) > B^2 > 0$. $(0, 0)$ is unstable and only $(0, \mu_1)$ exists.

We construct a bifurcation diagram on $B - E$ plane (see Fig. 10), which describes the above results and also the stability nature of origin. Two curves $(B - D - 1) = 0$ and $B^2 + 4C(1 + D)(B - D - 1) = 0$ divide the bifurcation diagram into three subregions and corresponding phase portraits are also shown in Fig. 11.

Hence, by blowing-down back (14)–(15), the line $u = 0$ is collapsed to the origin of the system (9)–(10). When $(0, \mu_{1,2})$ are stable, then invariant attracting curve is also mapped to an curve in the first quadrant which passes through the origin. So, the axial equilibrium point $E_0(0, 0)$ of the model (9)–(10) is stable at that region.

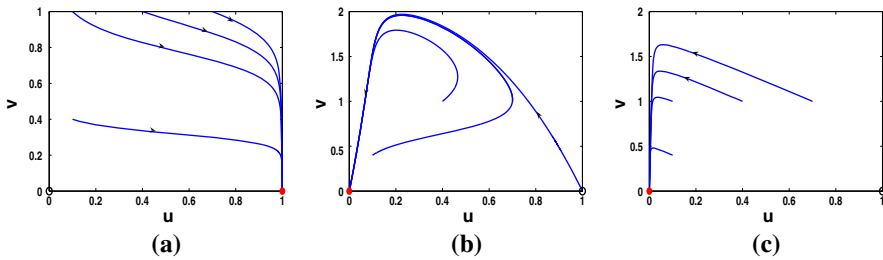


Fig. 11 Stability of $E_0(0,0)$ corresponding to Fig. 10. **a** for region A1, **b** for region A2, **(c)** for region A3

References

1. Aguirree, P., Flores, J.D., Olivares, E.: Bifurcations and global dynamics in a predator-prey model with a strong Allee effect on the prey and a ratio-dependent functional response (2014)
2. Allee, W.C.: *Animal Aggregations*. University of Chicago Press, Chicago (1931)
3. Angelis, D.: *Dynamics of Nutrient Cycling and Food Webs*. Chapman and Hall, London (1992)
4. Arditi, R., Perrin, N., Saiah, H.: Functional responses and heterogeneities: an experimental test with cladocerans. *Oikos* **60**, 69–75 (1991)
5. Arditi, R., Ginzbur, L.R.: Coupling in predator-prey dynamics: ratio-dependence. *J. Theor. Biol.* **139**, 311–326 (1989)
6. Banerjee, M., Petrovskii, S.: Self-organised spatial patterns and chaos in a ratio-dependent predator-prey system. *Theor. Ecol.* **4**, 37–53 (2011)
7. Bazykin, A.D., Khibnik, A.I., Krauskopf, B.: *Nonlinear dynamics of interacting populations*, Vol. 11 (World Scientific Publishing Company Incorporated) (1998)
8. Beddington, J.R.: Mutual interference between parasites or predators and its effect on searching efficiency. *J. Animal Ecol.* **44**, 331–340 (1975)
9. Beretta, E., Kuang, Y.: Global analyses in some delayed ratio-dependent predator prey systems. *Nonlinear Anal.* **32**, 381–408 (1998)
10. Berezovskaya, F., Karev, G., Arditi, R.: Parametric analysis of the ratio-dependent predator-prey model. *J. Math. Biol.* **43**, 221–246 (2001)
11. Canale, R.: Predator-prey relationships in a model for the activated process. *Biotechnol. Bioeng.* **11**, 887–907 (1969)
12. Conway, E.D., Smoller, J.A.: Global analysis of a system of predator-prey equations. *SIAM J. Appl. Math.* **46**, 630–642 (1986)
13. Courchamp, F., Clutton-brock, T., Grenfell, B.: Inverse density dependence and the Allee effect. *Trends Ecol. Evol.* **14**, 405–410 (1999)
14. DeAngelis, D.L., Goldstein, R.A., O'Neill, R.V.: A model for trophic interaction. *Ecology* **56**, 881–892 (1975)
15. Fan, Y.H., Li, W.T.: Permanence for a delayed discrete ratio-dependent predator-prey system with Holling type functional response. *J. Math. Anal. Appl.* **299**(2), 357–374 (2004)
16. Freedman, H.: Stability analysis of a predator-prey system with mutual interference and density-dependent death rates. *Bull. Math. Biol.* **41**, 67–78 (1979)
17. Freedman, H.: *Deterministic Mathematical Method in Population Ecology*. Dekker, New York (1990)
18. Gonzalez-Olivares, E., Rojas-Palma, A.: Multiple limit cycles in a gause type predator-prey model with holling type III functional response and Allee effect on prey. *Bull. Math. Biol.* **73**, 1378–1397 (2011)
19. Hanski, I.: The functional response of predators: worries about scale. *Trends Ecol. Evol.* **6**, 141–142 (1991)
20. Haque, M.: Ratio-dependent predator-prey models of interacting populations. *Bull. Math. Biol.* **71**, 430–452 (2009)
21. Hilker, F.: Population collapse to extinction: the catastrophic combination of parasitism and Allee effect. *J. Biol. Dyn.* **4**, 86–100 (2010)

22. Hilker, F., Langlais, Malchow H: The Allee effect and infectious diseases: extinction, multistability and the disappearance of oscillations. *Am. Nat.* **173**, 72–88 (2009)
23. Holling, C.: The functional response of predators to prey density and its role in mimicry and population regulation. *Mem. Entomol. Soc. Can.* **97**, 1–60 (1965)
24. Hsu, S., Hwang, T., Kuang, Y.: Global analysis of the michaelis-menten type ratio-dependent predator-prey system. *J. Math. Biol.* **42**, 489–506 (2001)
25. Jost, C., Arino, O., Arditi, R.: About deterministic extinction in ratio-dependent predator-prey models. *Bull. Math. Biol.* **61**, 19–32 (1999)
26. Kot, M.: *Elements of Mathematical Ecology*. Cambridge University Press, Cambridge (2001)
27. Garain, K., Mandal, P.S.: Bifurcation Analysis of a prey-predator model with Beddington-DeAngelis type functional response and Allee effect in prey, *International Journal of Bifurcation and Chaos*, 2018 (accepted)
28. Kuang, Y., Beretta, E.: Global qualitative analysis of a ratio-dependent predator-prey system. *J. Math. Biol.* **36**, 389–406 (1998)
29. Kuznetsov, Y.A.: *Elements of Applied Bifurcation Theory*. Springer, New York (2004)
30. Lotka, A.J.: *A Natural Population Norm i and ii*. Washington Academy of Sciences, Washington, DC (1913)
31. May, R.M.: *Stability and Complexity in Model Ecosystems*. Princeton University Press, New Jersey (2001)
32. McGehee, E.A., Schutt, N., Vasquez, D.A., Peacock-Lopez, E.: Bifurcations, and temporal and spatial patterns of a modified lotka-volterra model. *Int. J. Bifurc. Chaos* **18**, 2223–2248 (2008)
33. Morozov, A., Petrovskii, S., Li, B.L.: Spatiotemporal complexity of patchy invasion in a predator-prey system with the Allee effect. *J. Theor. Biol.* **238**, 18–35 (2006)
34. Pablo, A., Flores, J.D., Gonzalez-Olivares, E.: Bifurcations and global dynamics in a predator-prey model with a strong Allee effect on the prey and a ratio-dependent functional response. *Nonlinear Anal. Real World Appl.* **16**, 235–249 (2014)
35. Pal, P.J., Saha, T.: Dynamical complexity of a ratio-dependent predator-prey model with strong additive Allee effect. *Appl. Math.* **146**, 287–298 (2015)
36. Pal, P.J., Saha, T., Sen, M., Banerjee, M.: A delayed predator-prey model with strong Allee effect in prey population growth. *Nonlinear Dyn.* **68**, 23–42 (2012)
37. Perko, L.: *Differential Equations and Dynamical Systems*. Springer, New York (1991)
38. Sen, M., Morozov, A.: Bifurcation analysis of a ratio-dependent prey-predator model with the Allee effect. *Ecol. Complex.* **11**, 12–27 (2012)
39. Sen, M., Banerjee, M.: Rich global dynamics in a prey-predator model with Allee effect and density dependent death rate of predator. *Int. J. Bifurc. Chaos* **25**, 10 (2015)
40. Stephens, P., Sutherland, W.: Consequences of the Allee effect for behavior, ecology and conservation. *trends in ecology and evolutionl. Electron. J. Differ. Equ.* **14**, 401–405 (1999)
41. Volterra, V.: Fluctuations in the abundance of a species considered mathematically. *Nature* **118**, 558–560 (1926)
42. Voorn, G., Hemerik, L., Boer, M., Kooi, B.: Heteroclinic orbits indicate over exploitation in predator-prey systems with a strong Allee effect. *Math. Biosci.* **209**, 451–469 (2001)
43. Wng, L., Li, W.T.: Periodic solutions and permanence for a delayed nonautonomous ratiodependent predator-prey model with Holling type functional response. *J. Comput. Appl. Math.* **162**(2), 341–357 (2004)
44. Wang, M., Kot, M.: Speeds of invasion in a model with strong or weak Allee effects. *Math. Biosci.* **171**, 83–97 (2001)
45. Wang, J., Shi, J., Wei, J.: Predator-prey system with strong Allee effect in prey. *J. Math. Biol.* **62**, 291–331 (2011)
46. Xiao, D., Ruan, S.: Global dynamics of a ratio-dependent predator-prey system. *J. Math. Biol.* **43**, 268–290 (2001)